MODERN THEORY OF NUMERICAL METHODS FOR MOTION BY MEAN CURVATURE

by

Ryo Takei

B.Sc., Simon Fraser University, 2005

A THESIS SUBMITTED IN PARTIAL FULFILLMENT
OF THE REQUIREMENTS FOR THE DEGREE OF
MASTER OF SCIENCE
in the Department
of
Mathematics

SIMON FRASER UNIVERSITY
Summer 2007

APPROVAL

Name:	Ryo Takei
Degree:	Master of Science
Title of thesis:	Modern Theory of Numerical Methods for Motion by Mean Curvature
Examining Committee:	Dr. J.F. Williams Chair
	Dr. Adam Oberman, Senior Supervisor
	Dr. Steven Ruuth, Supervisor
	Dr. Ralf Wittenberg, Internal Examiner

Date Approved: July 3, 2007

Abstract

We analyze two finite difference schemes, the median and the morphological schemes, for numerically solving the motion by mean curvature partial differential equation. We show that these schemes satisfy sufficient conditions for convergence to the correct viscosity solution of the underlying equation. Moreover, we explore a recent link between the motion by mean curvature partial differential equation to a two-person differential game; we argue that these schemes can be interpreted as discrete approximations to this two-person differential game. Numerical results comparing the two schemes to standard finite difference discretizations are also presented.

Keywords:
Motion by mean curvature; Viscosity solutions; Two-person differential games; Degenerate elliptic schemes; Finite difference method

Acknowledgments

I would like to thank my senior supervisor, Dr. Adam Oberman, for sharing his passion for various topics in applied mathematics. I thank Dr. Steve Ruuth and Dr. JF Williams for their service in my committee, and Dr. Ralf Wittenberg for inviting me into the subject of applied mathematics. I would also like to thank the rest of the applied math faculty at Simon Fraser University for providing me a great intellectual atmosphere.

I am grateful for my colleagues at Simon Fraser University, especially Mr. Wilson Au for his prompt and knowlegeable help in MATLAB. I thank Mr. Au, Dr. Ian Mitchell and Dr. Shiro Ogawa for revising drafts of this report. Last but not least, I thank my family and friends for supporting me through various ways during my academic career.

I was financially supported by the National Science and Engineering Research Council (NSERC) of Canada as a USRA fellow (2005) and a CGS-M fellow (2006-2007), and Simon Fraser University during my undergraduate and graduate years. I humbly thank both for their generosity and hospitality.

Contents

List of Tables

List of Figures

Chapter 1

Introduction

Our goal in this thesis is to understand and interpret numerical schemes that solve the initial and boundary value problem,

$$\frac{\partial u(t,x,y)}{\partial t} = |\nabla u| \nabla \cdot \left(\frac{\nabla u}{\nabla u|} \right) \qquad \text{for } (t,x,y) \in [0,T) \times \Omega \tag{1.1}$$

$$u(t,x,y) = f(t,x,y) \qquad \text{on } (t,x,y) \in [0,T) \times \partial\Omega \tag{1.2}$$

$$u(0,x,y) = u_0(x,y) \qquad \text{on } (x,y) \in \Omega, \tag{1.3}$$

for a domain $\Omega \subset \mathbb{R}^2$ and some $T > 0$. More precisely, we study

1. sufficient criteria for numerically capturing the correct weak solution, the *viscosity solution* (see Chapter 2), of (1.1), and

2. how to construct and interpret numerical schemes for (1.1) via a differential game theory (see Chapter 3) approach.

We will refer to the partial differential equation in (1.1) as *motion by mean curvature*. As the name suggests, the problem (1.1), (1.2), (1.3) is closely related to the problem of evolving contours according to their curvature. This geometric meaning of (1.1) is helpful when constructing weak solutions. We will establish this link in Section 1.2.

1.1 Curvature Motion

The central theme of this thesis is the evolution of curves in two dimensions driven by their curvature. More precisely, in two dimensions, if we denote by $\mathcal{C}(t,s) \in \mathbb{R}^2$ the set of points

in the plane representing some curve parametrized by s at time t, we wish to evolve it by

$$\frac{\partial \mathcal{C}}{\partial t}(t,s) = \kappa(t,s)\hat{\mathcal{N}}(t,s), \tag{1.4}$$

$$\mathcal{C}(t,s) = \mathcal{C}_0(s) \tag{1.5}$$

where κ is the mean curvature and $\hat{\mathcal{N}}$ the unit inward normal of $\mathcal{C}$ at (t,s).

Recently, curvature motion has proved useful in image processing problems, such as denoising. Other areas of application include fluid dynamics, combustion, crystal growth and front propagation.

1.2 Level Set Formulation

The level set method, invented by Osher and Sethian [20], has proved to be one of the most versatile and robust methods to evolve curves and surfaces, both in theoretical and numerical settings. The basic idea is to represent a given curve by a zero level set of a surface. By increasing the co-dimension one can treat a wide class of curve evolution problems naturally. For example, kinks and topological changes of a curve are considered to be computationally difficult to tame using direct numerical methods for (1.4), but are easily implemented using the level set method. For an overview of other curve evolving methods, such as marker-point methods and volume preserving methods, see [23].

We briefly develop the level set formulation of curve evolution in $\mathbb{R}^2$; the same idea extends to higher dimensions. Suppose we start with (1.4), but with κ replaced by an arbitrary normal velocity vector $v(t,s)$:

$$\frac{\partial \mathcal{C}}{\partial t}(t,s) = v(t,s)\hat{\mathcal{N}}(t,s) \tag{1.6}$$

Define the *embedding function* $u : [0,T) \times \mathbb{R}^2 \to \mathbb{R}$ to be the surface that will represent $\mathcal{C}$ by its zero level set. This is equivalent to saying, if we define

$$\mathcal{L}_c(t,x,y) = \{(x,y) : u(t,x,y) = c\}, \tag{1.7}$$

then $\mathcal{C}(t,x,y) = \mathcal{L}_0(t,x,y)$. Now if we take the derivative with respect to t of $0 = u(t,x,y)$, ie. the equation satisfying the coordinates of the points on $\mathcal{C}$, we have

$$0 = \frac{d}{dt}u(t,x,y) = \nabla u(t,\mathcal{L}_0) \cdot \frac{\partial \mathcal{L}_0}{\partial t} + \frac{\partial u}{\partial t}(t,\mathcal{L}_0). \tag{1.8}$$

Noting that

$$\frac{\partial \mathcal{L}_0}{\partial t} = \frac{\partial \mathcal{C}}{\partial t} = v\hat{\mathcal{N}}, \tag{1.9}$$

we continue from (1.8):

$$\begin{aligned} 0 &= \nabla u(t, \mathcal{L}_0) \cdot \hat{\mathcal{N}} v + \frac{\partial u}{\partial t} && (1.10)\\ &= -v|\nabla u(t, \mathcal{L}_0)|\hat{\mathcal{N}} \cdot \hat{\mathcal{N}} + \frac{\partial u}{\partial t} && (1.11)\\ &= -v|\nabla u(t, \mathcal{L}_0)| + \frac{\partial u}{\partial t}, && (1.12) \end{aligned}$$

since $\nabla u(t, \mathcal{L}_0)$ points in the opposite direction of $\hat{\mathcal{N}}$. The norm $|\cdot|$ is the usual Euclidean norm. We need not necessarily take the zero level set; hence, we can replace $\mathcal{L}_0$ by $\mathcal{L}_c$ for any c. But, since any point $(x, y) \in \mathbb{R}^2$ must be on *some* level set of u, we can replace $\mathcal{L}_0$ simply by (x, y). After this replacement, we arrive at

$$\frac{\partial u}{\partial t}(t, x, y) = v|\nabla u(t, x, y)|. \tag{1.13}$$

The partial differential equation (1.13) is the *level set formulation* of the curve evolution problem (1.6). For motion by mean curvature, we have

$$v(t, s) = \kappa(t, s) = \nabla \cdot \left(\frac{\nabla u}{|\nabla u|} \right),$$

and hence (1.1) is the level set formulation of (1.4).

1.2.1 Other Representations of Motion by Mean Curvature

In understanding (1.1), it is useful to be familiar with other forms of motion by mean curvature. Expanding and simplifying the right hand side of (1.1) yields

$$\frac{\partial u}{\partial t} = \frac{u_y^2 u_{xx} - 2u_x u_y u_{xy} + u_x^2 u_{yy}}{u_x^2 + u_y^2}. \tag{1.14}$$

Now we turn to a more geometric representation. The Laplacian operator Δ may be decomposed as follows:

$$\Delta u = \mathbf{n}^T (D^2 u)\mathbf{n} + \mathbf{t}^T (D^2 u)\mathbf{t} \tag{1.15}$$

where $\mathbf{n} = \nabla u/|\nabla u|$, $\mathbf{t} = \nabla^\perp u/|\nabla u|$ and $D^2 u$ is the Hessian of u. ($\nabla^\perp$ is the operator $(\frac{\partial}{\partial y}, -\frac{\partial}{\partial x})$.) This decomposition separates an isotropic second derivative, the Laplacian,

into second derivatives in the normal and tangent directions of the level set contours of u, $\mathbf{n}$ and $\mathbf{t}$, respectively. Hence, a more suggestive form of (1.15) may be

$$\Delta u = \frac{\partial^2 u}{\partial \mathbf{n}^2} + \frac{\partial^2 u}{\partial \mathbf{t}^2}. \tag{1.16}$$

The two terms on the right hand side of (1.15) and (1.16) are referred to as the *infinity Laplacian* of u denoted by $\Delta_\infty u$, and the *1-Laplacian* of u denoted by $\Delta_1 u$, respectively[1]. This decomposition into two orthogonal directions is special to $\mathbb{R}^2$. But $\Delta_1 u$ in fact equals the right hand side of (1.1). Hence, motion by mean curvature (1.1) may also be represented in the following way:

$$\begin{aligned} \frac{\partial u}{\partial t} &= \Delta_1 u & (1.17)\\ &= \Delta u - \Delta_\infty u & (1.18)\\ &= \frac{\partial^2 u}{\partial \mathbf{t}^2}. & (1.19) \end{aligned}$$

1.2.2 Remarks

1. The final step leading to (1.13) tells us an interesting fact: by solving (1.13), one is solving (1.4) for *every* level set of the embedding function u.

2. A theorem of Grayson [11] states that for all closed simple $\mathcal{C}_0$ in $\mathbb{R}^2$, a curve $\mathcal{C}$ evolving according to (1.4) eventually shrinks to a point, and then disappears. This is *not* the case in higher dimensions. For example, a "dumbbell" shaped surface in $\mathbb{R}^3$ may have its "handle" pinch off to cause a change in topology, see Figure 1.1.

3. The representation (1.19) clarifies what it means to evolve the embedding function u by motion by mean curvature: an anisotropic Gaussian smoothing restricted to each level set[2].

1.3 Layout of the Thesis

Much of this thesis will be devoted towards developing the necessary tools. This is due to the author's philosophy that numerical simulations should only be attacked when the underlying partial differential equation and its numerical theory are sufficiently understood.

[1] This notation is not standard. Some authors define $\Delta_1 u$ as our definition of $\Delta_1 u$ multiplied by some power of $|\nabla u|$.

[2] This happens to be a very useful property of motion by mean curvature in image denoising.

Figure 1.1: The evolution of a "dumbbell". Left to right: Initial surface; the surface evolved after some time $t > 0$. (Numerical code courtesy of Mr. Wilson Au.)

Chapter 2 defines and outlines major results of viscosity solutions for (1.1). This chapter contains mainly theoretical results and properties which will later be used to evaluate numerical schemes. Chapter 3 presents the two-person differential game interpretation of (1.1), (1.3). The interpretation is included in this thesis to shed new light on modern numerical schemes for (1.1). Chapter 4 develops the modern machinery needed to prove convergence of schemes to the correct weak solution. Chapter 5 presents two modern finite difference schemes for (1.1). It also gives proofs of convergence and numerical results. Chapter 6 empirically compares these schemes to standard finite difference schemes on several test cases.

Chapter 2

Viscosity Solutions

The notion of *viscosity solutions* provides a powerful framework for proving the existence and uniqueness of weak solutions for a wide class of partial differential equations. The idea is to give suitable conditions to allow for non-smooth solutions while achieving existence and uniqueness. One allows of non-smoothness, roughly speaking, by touching the weak solution u from above and below by C^∞ test functions ϕ and applying derivatives on ϕ rather than on u.

Viscosity solutions were first developed for first order Hamilton-Jacobi type equations[1] by Crandall and Lions in 1983; similar theory for motion by mean curvature (1.1) was later introduced by Evans and Spruck [7] and Chen, Giga and Goto [3]. We will mainly follow the development of the theory as introduced by Evans and Spruck.

2.1 Definitions

For this section, we will use the forms,

$$u_t = \Delta u - \frac{1}{|\nabla u|^2}(\nabla u)^T D^2 u \nabla u \qquad \mathbb{R}^2 \times [0,\infty) \tag{2.1}$$

and,

$$u_t = \frac{1}{|\nabla u|^2}(\nabla^\perp u)^T D^2 u \ \nabla^\perp u \qquad \mathbb{R}^2 \times [0,\infty) \tag{2.2}$$

for motion by mean curvature, where $\nabla^\perp$ is the operator $(\frac{\partial}{\partial y}, -\frac{\partial}{\partial x})$ and $D^2 u$ is the Hessian of u. These are of the same form as (1.18) and (1.17), respectively.

[1] For a definition of Hamilton-Jacobi equations and its derivatives, see [6]

2.1.1 Degenerate Ellipticity

Let S^2 be the set of 2 by 2 symmetric real matrices and Ω be a domain in $\mathbb{R}^2$. We start by defining a class of *degenerate elliptic partial differential equations.*

Definition 2.1.1 (Degenerate ellipticity). *Let*

$$F(x, p, X) : \Omega \times \mathbb{R}^2 \times S^2 \to \mathbb{R}$$

be continuous. Denote $F[u](x) := F(x, \nabla u(x), D^2 u)$ *for some smooth function* u. *Consider the elliptic and parabolic Dirichlet boundary value problems,*

$$\begin{cases} F[u](x) = 0 & x \in \Omega \\ u(x) = g(x) & x \in \partial\Omega, \end{cases} \tag{2.3}$$

and

$$\begin{cases} u_t(t,x) + F[u](t,x) = 0 & (t,x) \in [0,T) \times \Omega \\ u(t,x) = g(t,x) & (t,x) \in \{t=0\} \times \Omega \bigcup [0,T) \times \partial\Omega. \end{cases} \tag{2.4}$$

We say that (2.3) or (2.4) is degenerate elliptic *if*

$$F(x, p, X) \leq F(x, p, Y) \text{ whenever } Y \leq X. \tag{2.5}$$

Note that by $X \leq Y$ for matrices X, Y, we mean that $(Y - X)$ is a positive semi-definite matrix. We show that motion by mean curvature is degenerate elliptic. The continuity of F in the preceding definition may be relaxed by taking its upper and lower semicontinous functions; this allows the development of the forthcoming theory also at isolated discontinuities.

Proposition 2.1.2. *Motion by mean curvature (2.2) is degenerate elliptic.*

Proof. In this case, the function F is

$$F(x, p, X) = F(p, X) = -\frac{1}{|p|^2}(p^\perp)^T X \; p^\perp, \tag{2.6}$$

where F is continuous except at an isolated point $p = 0$, which poses no problems. We assume that $p \neq 0$. If $Y \leq X$, then

$$F(p, X) - F(p, Y) = -\frac{1}{|p|^2}(p^\perp)^T (X - Y) \; p^\perp \leq 0, \tag{2.7}$$

since $(X - Y)$ is positive semi-definite. □

As mentioned in the beginning of the chapter, the goal is to allow for 'suitable' non-smooth (but continuous) solutions to satisfy (2.1), or equivalently, (2.2). We will later clarify what is meant by 'suitable'. The immediate problem is how one should deal with ∇u and D^2u, if u were not smooth.

2.1.2 Viscosity Solutions

To motivate the definition of viscosity solutions, we introduce an arbitrary test function $\phi \in C^\infty((0,T) \times \Omega)$ and for the time being, suppose $u \in C^2((0,T) \times \Omega)$ satisfies the inequality

$$u_t + F(\nabla u, D^2 u) \leq 0. \tag{2.8}$$

Such u is called a *subsolution* of (2.4). Suppose $(u - \phi)$ attains a local maximum at the point and time $z_0 = (t_0, x_0, y_0) \in (0,T) \times \Omega$. Then, by calculus, we have,

$$u_t(z_0) = \phi_t(z_0), \quad \nabla u(z_0) = \nabla \phi(z_0), \quad D^2 u(z_0) \leq D^2 \phi(z_0).$$

If F is defined as in (2.6), since motion by mean curvature is degenerate elliptic,

$$\phi_t + F(\nabla \phi, D^2 \phi) \leq u_t + F(\nabla u, D^2 u) \leq 0 \tag{2.9}$$

at z_0. Hence, we may characterize solutions that satisfy (2.8) by a differential inequality involving derivatives just in test functions:

$$\phi_t + F(\nabla \phi, D^2 \phi) \leq 0 \qquad \text{at } z_0. \tag{2.10}$$

If we assume, without loss of generality, that $u(z_0) = \phi(z_0)$, then the test function can be interpreted as "touching the solution u from above" at the point and time z_0 [6, Lemma p. 544]. Assuming that $(u - \phi)$ now has a local minimum, reversing the inequality in (2.8) (u is then called a *supersolution*) also reverses the inequality in (2.10). Subsequently, if both inequalities hold, and F is chosen as in Proposition 2.1.2, we have a solution to (2.1).
We now give definitions of *viscosity subsolutions* and *viscosity supersolutions* [2].

Definition 2.1.3 (Viscosity subsolution). *A bounded function $u \in C(\Omega \times [0,\infty))$ is a* viscosity subsolution *of (2.1), provided that if $(u - \phi)$ has a local maximum at a point (t_0, x_0, y_0) for a smooth ϕ, then,*

[2] In [7], what we call viscosity solutions are referred to as "weak solutions"

1. *if* $\nabla\phi(t_0, x_0, y_0) \neq 0$, *then*

$$\phi_t \leq \Delta\phi - \frac{1}{|\nabla\phi|^2}(\nabla\phi)^T D^2\phi \nabla\phi \tag{2.11}$$

at (t_0, x_0, y_0), *or,*

2. *if* $\nabla\phi(t_0, x_0, y_0) = 0$, *then*

$$\phi_t \leq \Delta\phi - \eta^T D^2\phi\ \eta \tag{2.12}$$

at (t_0, x_0, y_0), *for some* $\eta \in \mathbb{R}^2$ *such that* $|\eta| \leq 1$.

Definition 2.1.4 (Viscosity supersolution). *A bounded function* $u \in C(\Omega \times [0, \infty))$ *is a* viscosity supersolution *of (2.1), provided that if* $(u - \phi)$ *has a local minimum at a point* (t_0, x_0, y_0) *for a smooth* ϕ, *then,*

1. *if* $\nabla\phi(t_0, x_0, y_0) \neq 0$, *then*

$$\phi_t \geq \Delta\phi - \frac{1}{|\nabla\phi|^2}(\nabla\phi)^T D^2\phi \nabla\phi \tag{2.13}$$

at (t_0, x_0, y_0), *or,*

2. *if* $\nabla\phi(t_0, x_0, y_0) = 0$, *then*

$$\phi_t \geq \Delta\phi - \eta^T D^2\phi\ \eta \tag{2.14}$$

at (t_0, x_0, y_0), *for some* $\eta \in \mathbb{R}^2$ *such that* $|\eta| \leq 1$.

The definition for *viscosity solutions* follows.

Definition 2.1.5 (Viscosity solution). *A bounded function* $u \in C(\Omega \times [0, \infty))$ *is a* viscosity solution *of (2.1), if it is both a viscosity subsolution and a viscosity supersolution.*

See [9, Chapter 2] for a simpler definition of viscosity solutions (Definitions 2.1.3, 2.1.4 and 2.1.5) using upper and lower semicontinuous functions. Note that in definitions 2.1.3 and 2.1.4, there is a degree of freedom on η where the gradient vanishes. The conditions on $|\eta|$ in (2.12) and (2.14) are particularly tailored for useful convergence properties of viscosity solutions; see, for example, [7, Theorem 2.7].

The form (2.12) and (2.14) can be slightly simplified. We apply a generalization of (1.15). By letting $\nu = \eta^\perp$, (2.12) can be written as

$$\phi_t \leq \nu^T D^2\phi\ \nu, \tag{2.15}$$

and $|\nu| \leq 1$, and similarly for (2.14) with reversed inequality.

2.1.3 Properties of Viscosity Solutions

We outline three fundamental properties of viscosity solutions for (2.1): the comparison property, uniqueness and existence. Some of these will be motivated, but all will be given without proof. For rigorous justification, we refer the reader to [7] or [9]. We also prove a Lemma connecting viscosity solutions to classical solutions of (2.1).

First, we present the comparison property.

Theorem 2.1.6 (Comparison property). *Let u and v be a viscosity subsolution and supersolution, respectively, of (2.1), such that $u \leq v$ in $\{t = 0\} \times \Omega$. Assume further that*

$$\text{on } [0,\infty) \times \Omega \bigcap \{\sqrt{x^2+y^2} + t \geq R\},\ u \text{ and } v \text{ are constants such that } u \leq v \tag{2.16}$$

for some $R \geq 0$. Then,

$$u \leq v \qquad \text{on } [0,\infty) \times \Omega. \tag{2.17}$$

The comparison principle is a nonlinear generalization of the maximum principle for the heat equation. Recall that the (strong) maximum principle asserts the maximum of a solution to the heat equation (only) occurs either at the initial condition or on the boundary of the domain.

Consider now motion by mean curvature (2.1). As shown in Example 2.2.1 below, a constant is a viscosity sub- and supersolution of (2.1) that satisfies the assumptions of Theorem 2.1.6. If u is a viscosity solution of (2.1) bounded above by c_1 and below by c_2 at $t = 0$, then Theorem 2.1.6 implies that $c_1 \leq u \leq c_2$ for all $t \geq 0$. We have shown the *contraction property*, or the *non-expansivity in the ∞-norm*:

Theorem 2.1.7 (Contraction property). *Let u, v be viscosity solutions of (2.1), such that (2.16) holds for some $R > 0$. Then*

$$\max_{0 \leq t < \infty} ||u(t,\cdot,\cdot) - v(t,\cdot,\cdot)||_{L^\infty(\mathbb{R}^2)} = ||u(0,\cdot,\cdot) - v(0,\cdot,\cdot)||_{L^\infty(\mathbb{R}^2)} \tag{2.18}$$

Suppose now that u and v are two viscosity solutions to (2.1) with the same initial condition. Suppose further that u and v both satisfy (2.16). Since both are viscosity sub- and supersolutions, and $u \leq v$ and $v \leq u$ at $t = 0$, the Theorem 2.1.6 implies that $u \leq v$ and $v \leq u$ for all $t \geq 0$. Hence, the comparison principle implies the following:

Theorem 2.1.8 (Uniqueness of viscosity solutions). *A viscosity solution of (2.1) is unique if it is constant on $\Omega \times [0,\infty) \bigcap \{\sqrt{x^2+y^2} + t \geq R\}$.*

Finally, we present the existence result:

Theorem 2.1.9 (Existence of viscosity solutions). *Suppose $g : \Omega \to \mathbb{R}$ is a continuous function such that*

$$g \text{ is constant on } \Omega \bigcap \{\sqrt{x^2+y^2} \geq S\}. \tag{2.19}$$

for some $S > 0$. Then there exists a viscosity solution u of (2.1) such that $u(0,x,y) = g(x,y)$ and is constant on $\Omega \times [0,\infty) \bigcap \{\sqrt{x^2+y^2}+t \geq R\}$. The constant R only depends on S.

Any form of weak solution must coincide with the classical solution whenever sufficient smoothness is met. In the case of (2.1), C^2 is sufficient.

Lemma 2.1.10. *A classical solution $u \in C^2([0,T] \times \Omega)$ of (2.1) is a viscosity solution.*

Proof. Suppose u is C^2 and satisfies (2.1) in the classical sense at $z_0 = (t_0, x_0, y_0)$, so $\nabla u(z_0) \neq 0$. First we show that u is a subsolution. Suppose $(u - \phi)$ has a local maximum at z_0 for some smooth ϕ. Then $u_t(z_0) = \phi_t(z_0)$, $\nabla u(z_0) = \nabla \phi(z_0)$ and $D^2 u(z_0) \leq D^2 \phi(z_0)$. By Proposition 2.1.2, (2.1) is degenerate elliptic. Defining F as in (2.6), combining the results gives

$$-\phi_t(z_0) = -u_t(z_0) = F(\nabla u(z_0), D^2 u(z_0)) \geq F(\nabla \phi(z_0), D^2 \phi(z_0)) \tag{2.20}$$

and we are done. The argument for u being a supersolution reverses the inequalities above. Hence, u is a viscosity solution. □

We remark on a result useful when constructing new solutions from known ones.

Lemma 2.1.11. *If u_1 and u_2 are viscosity solutions of (2.1) then $u = \min\{u_1, u_2\}$ is a viscosity supersolution of (2.1).*

Proof. If $(u - \phi)$ has a local minimum at $z_0 = (t_0, x_0, y_0)$, then $\min\{u_1 - \phi, u_2 - \phi\}$ does also. Then either $(u_1 - \phi)$ or $(u_2 - \phi)$ has a local minimum at z_0. But since u_1, u_2 are viscosity solutions, we have that ϕ satisfies (2.13) at z_0. The case when $\nabla \phi = 0$ is a weaker condition, so the argument holds. □

2.2 Interpretations and Examples

Motivation and definitions of viscosity solutions thus far have been analytic. We now provide a geometric interpretation of why the definitions of viscosity sub- and supersolutions are

plausible. In doing so, we remind the reader of the geometric meaning of (2.1): motion of level sets in the inward normal direction by their curvature.

Suppose u, ϕ are smooth and convex, and $(u - \phi)$ attains a maximum at x_0 and time t. This is the case where u is a viscosity subsolution. The level sets of u and ϕ, geometrically, are shown in Figure 2.1. Let κ_u and κ_ϕ denote the curvature of the level sets at x_0 of u and ϕ, respectively. Clearly, $\kappa_u \leq \kappa_\phi$. Furthermore, since $|\nabla u| = |\nabla \phi|$, we have that $\Delta_1 u \leq \Delta_1 \phi$, at x_0. Therefore,

$$\phi_t = u_t = \Delta_1 u \leq \Delta_1 \phi,$$

which is equivalent to (2.11).

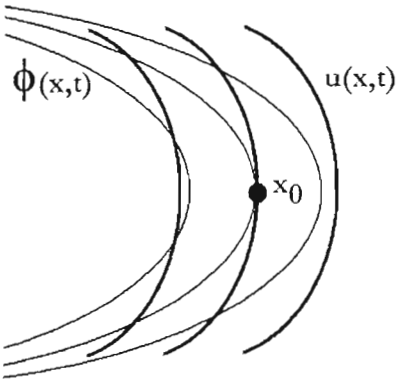

Figure 2.1: Visualization of viscosity subsolution. The level sets of u and ϕ are shown in thick and thin lines, respectively. The function $(u - \phi)$ attains a maximum at the point x_0.

The same argument can be made when $(u - \phi)$ attains a minimum at x_0 and t. This is the case where u is a viscosity supersolution. The corresponding plot is shown in Figure 2.2.

For concreteness, we illustrate the definitions with three examples.

Example 2.2.1 (A constant). Consider the case $u = c$, a constant. Note that $u_t = \Delta u = 0$.

We first check that u is a viscosity subsolution according to Definition 2.1.3. Take any arbitrary point $z_0 = (t_0, x_0, y_0) \in [0, \infty) \times \Omega$. If $(u - \phi)$ has a local maximum, then $(u - \phi)_t = 0$ and $\Delta(u - \phi) \leq 0$, so $\phi_t = 0$ and $\Delta\phi \geq 0$. Choosing $\eta = 0$, we have (2.12), and we are done.

We next check that u is a viscosity supersolution according to Definition 2.1.4. If $(u - \phi)$

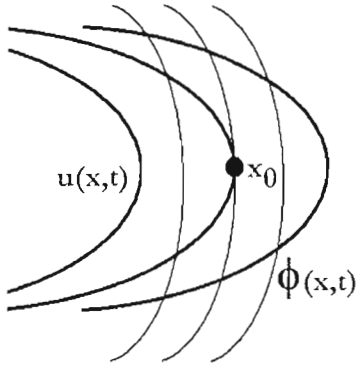

Figure 2.2: Visualization of viscosity supersolution. The level sets of u and ϕ are shown in thick and thin lines, respectively. The function $(u - \phi)$ attains a minimum at the point x_0.

has a local minimum, then $(u - \phi)_t = 0$ and $\Delta(u - \phi) \geq 0$, so $\phi_t = 0$ and $\Delta\phi \leq 0$. Again, choosing $\eta = 0$, we have (2.14), and we are done.

Since u is a viscosity subsolution and a viscosity supersolution, it is a viscosity solution.

Example 2.2.2 (A paraboloid). Let

$$u(t, x, y) = \frac{x^2 + y^2 - 1}{2} + t.$$

It is easy to check that u satisfies (2.1) in the classical sense at all points except at the origin. By Lemma 2.1.10, u is a viscosity solution except at the origin.

To check that u is a viscosity subsolution at the origin, if $(u - \phi)$ has a local maximum at $z_0 = (t_0, 0, 0)$, then $\phi_t(z_0) = u_t(z_0) = 1$, $\nabla\phi(z_0) = \nabla u(z_0) = 0$ and $\Delta\phi(z_0) \geq \Delta u(z_0) = 2$. So (2.12) is satisfied when $\eta = 0$.

To check that u is a viscosity supersolution at the origin, we use (2.15). If $(u - \phi)$ has a local minimum at $z_0 = (t_0, 0, 0)$, then $\phi_t(z_0) = u_t(z_0) = 1$. Choosing $\nu = 0$ satisfies the reverse inequality of (2.15).

Our last example is less trivial.

Example 2.2.3. Consider the function

$$u(t, x, y) = \min\left\{\frac{x^2 + y^2 - 1}{2} + t, 0\right\}. \tag{2.21}$$

At some $t_0 \geq 0$, u is a viscosity solution of (2.1) in the regions $S_1 := \{(x, y) : (x^2 + y^2 - 1)/2 + t_0 < 0\}$ and $S_2 := \{(x, y) : (x^2 + y^2 - 1)/2 + t_0 > 0\}$ by Examples 2.2.1 and 2.2.2, respectively. Furthermore, by Lemma 2.1.11, u is a supersolution of (2.1).

We argue geometrically that u is a viscosity subsolution in $S_3 := \{(x,y) : (x^2+y^2-1)/2+t_0 = 0\}$. Note that $\Delta_1 u = 1$ in S_1 and $\Delta_1 u = 0$ in S_2, the latter in the viscosity sense. Now, if $(u-\phi)$ attains a maximum for some smooth ϕ, the zero level set of ϕ must have a larger curvature in the inward normal direction than $1 = \Delta_1 u|_{S_1} > \Delta_1 u|_{S_2} = 0$. Hence, $\Delta_1 \phi \geq \max\{\Delta_1 u|_{S_1}, \Delta_1 u|_{S_2}\} \geq u_t = \phi_t$ in the viscosity sense on S_3. Thus u is a viscosity subsolution.

2.3 Further Interesting Properties

Recall that for the heat equation, information is propagated isotropically at "infinite speed". Observing the form (1.19), motion by mean curvature is effectively solving the heat equation along the direction tangent to the level set curves. We therefore naturally expect a property that propagates information at infinite speed for motion by mean curvature. More concretely, suppose two closed simple contours $\mathcal{C}$ and $\hat{\mathcal{C}}$ are evolved up to some arbitrary small time $t > 0$ to $\mathcal{C}_t$ and $\hat{\mathcal{C}}_t$, respectively. Evans and Spruck [7] presented the following result:

Theorem 2.3.1. *Denote by inside($\mathcal{C}$) the points in and on a closed simple contour $\mathcal{C}$. If inside($\mathcal{C}$) $\subset$ inside($\hat{\mathcal{C}}$) then inside($\mathcal{C}_t$) $\subset$ inside($\hat{\mathcal{C}}_t$) for all $t > 0$. Furthermore, if $\mathcal{C} \neq \hat{\mathcal{C}}$ then $\mathcal{C}_t \bigcap \hat{\mathcal{C}}_t = \emptyset$ for all $t > 0$.*

We show a simple consequence of this result. Suppose $\mathcal{C}$ and $\hat{\mathcal{C}}$ are convex and nearly identical, except for an "inward dent" on $\hat{\mathcal{C}}$ of arbitrary smallness. Theorem 2.3.1 asserts that for arbitrary small time $t > 0$, $\hat{\mathcal{C}}_t$ will be completely inside the open set with boundary $\mathcal{C}_t$ (Figure 2.3)! In other words, the difference in mean curvature locally propagated at infinite speed to the whole level set.

We now turn to a more bizarre phenomenon. Consider evolving a surface $u : [0,\infty)\times\Omega \to \mathbb{R}$ whose zero level sets are the x and y axes, as in Figure 2.4 (a). To see how this curve will evolve by (1.4), observe how an L-shaped initial curve will evolve, as shown in Figure 2.5. Since Γ_0 in Figure 2.4 (a) is four L-shaped curves rotated and superimposed, one would expect the curve to extend outward from the origin in *all* directions! If u is the underlying level set function, we see that its zero level set gets pulled apart from its origin. Consequently, an interior or a "fat" zero level set is formed for some finite time $t > 0$.

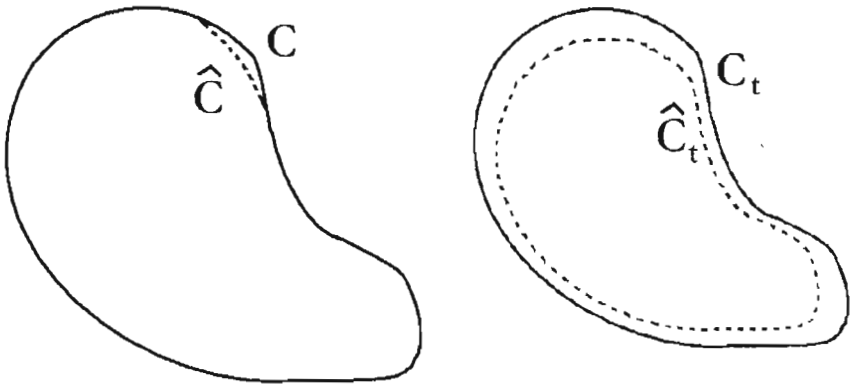

Figure 2.3: Example of infinite speed propagation. Left to right: Two nearly identical closed curves; the two curves after evolving for an arbitrary small time $t > 0$.

Graphically, the shaded region and its boundary in Figure 2.4 (b) is the zero level set Γ_t at $t > 0$. This is the correct viscosity solution for the given initial condition.

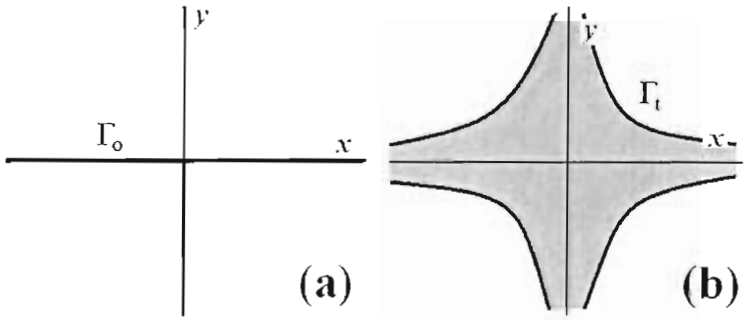

Figure 2.4: Fattening example. (a) Initial curve Γ_0; (b) the curve Γ_0 after evolving according to (1.1) for some finite time to give Γ_t.

2.4 Remarks

The definitions and results presented in this chapter were developed solely to supplement the following chapters and are by no means complete. For alternate definitions, complete proofs and other auxiliary results regarding viscosity solutions of motion by mean curvature

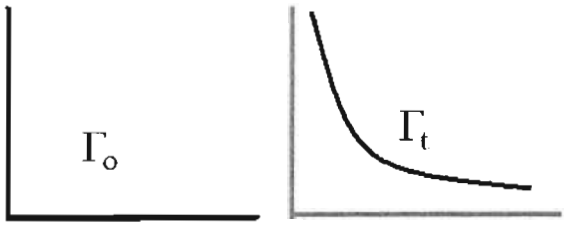

Figure 2.5: Evolution of a 'corner'. Left to right: Initial curve Γ_0; the curve Γ_0, shown in gray, after evolving according to (1.1) for some finite time to give Γ_t.

see [7], [3]. For a more comprehensive (and highly rigorous) overview of level set evolution equations, see [9].

Sources that verify fattening numerically and theoretically are outlined in [9].

Chapter 3

Differential Game Interpretations

Kohn and Serfaty [14] discovered that (1.1) can be interpreted as a solution to a *two-person differential game*. A game, in our sense, consists of a *value function* to be optimized under some rules represented as a mathematical condition. A two-person differential game is a game involving two opposing players – one that attempts to optimize some value function, and another that acts against it – that evolves continuously in real space and, and if relevant, in time. Rather than discussing further generalities, we will only present materials relevant to the following sections. For completeness, relevant theorems will be presented at the end of the section.

3.1 Example

As an illustration, we start with an example of a discrete time game. In the context of games, the two players will always be Paul and Carol.

Game 1 (Discrete convex minimum-time exit). *Let Ω be a bounded, convex set in $\mathbb{R}^2$, and $\varepsilon > 0$. Paul starts at some location $x \in \Omega$ and wishes to reach $\partial\Omega$ in a minimum number of steps; Carol is trying to obstruct him. The rules at each time step, in order, are:*

1. *Paul chooses a direction to move, by a unit vector $v \in \mathbb{R}^2$.*
2. *Carol chooses to reverse v or to leave it alone. i.e. she chooses $b = 1$ or -1 and replaces v by bv.*
3. *Paul moves in the direction bv by $\sqrt{2}\varepsilon$.*

Game 1 is referred to as an *exit game*, since exiting Ω is equivalent to Paul fulfilling his goal.

Can Paul exit in a finite number of steps? If Paul points v partially in the direction of closest exit, he knows that Carol will reverse it. On the other hand, if he decides to point v partially in the opposite direction to the closest exit, he knows she will leave v unaltered. The only advantageous direction Paul has left to move is in the *tangent direction* with respect to $\partial\Omega$ of the closest exit point - then Carol (and Paul) has no advantage (disadvantage) in reversing v or not. Meanwhile, since Ω is convex, Paul moves closer to $\partial\Omega$ at each step!

It is clear that, if Paul had started close enough to $\partial\Omega$, he can exit in one step by applying the aforementioned strategy. Let's define a closed curve $\partial\Omega_1 \subset \Omega$ such that, if Paul starts anywhere in the region $\Omega_1 = \{\text{area bounded by } \partial\Omega_1 \text{ and } \partial\Omega\}$, he can exit in one step, as shown in Figure 3.1. Likewise, define $\partial\Omega_{n+1}$ lying inside Ω_n such that Paul can exit Ω_n if he had started anywhere in the region $\Omega_{n+1} = \{\text{area bounded by } \partial\Omega_{n+1} \text{ and } \partial\Omega_n\}$, for $n = 1, 2, \ldots$. Then we have a finite set of concentric regions Ω_i that partition Ω. Hence, if Paul starts the game at $x \in \Omega_i$ an optimal strategy should exit him in exactly i steps.

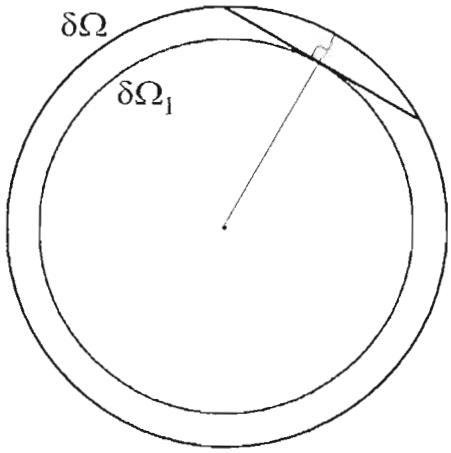

Figure 3.1: Paul can exit in one step if he is between $\partial\Omega_1$ and $\partial\Omega$. The distance he travels is $\sqrt{2}\varepsilon$ in the tangent direction to $\partial\Omega$.

This can be mathematically formulated as shown in the following section.

3.1.1 The Dynamic Programming Principle

Let the *value function* be $u^\varepsilon(x) = \varepsilon^2 k$ if:

Paul needs k steps to exit, starting from x and following an optimal strategy.

Then,

$$u^\varepsilon(x) = \min_{||v||=1} \max_{b=\pm 1} \{\varepsilon^2 + u^\varepsilon(x + \sqrt{2}\varepsilon b v)\}. \tag{3.1}$$

In other words, *the partial optimal strategy can be optimally extended locally.* This principle, in general, is known as the *dynamic programming principle.* The order of the min and max is important in (3.1) – Paul plans his strategy knowing that Carol would work optimally to obstruct him.

The equation derived from the dynamic programming principle (3.1) is key to deriving the partial differential equation for the continuous analogue of Game 1. From the definition of u^ε, $\sqrt{2}\varepsilon$ is the distance traveled by Paul at each step; hence, to derive the continuous game, we need to take the limit $\varepsilon \to 0$ of (3.1), in some sensible way. We will present here (and later for other games) heuristic arguments in deriving the corresponding partial differential equation; for rigorous proofs, see [14].

Let $u := \lim_{\varepsilon \to 0} u^\varepsilon$ uniformly, assuming such a limit exists. Then (3.1) suggests that,

$$u(x) \approx \min_{||v||=1} \max_{b=\pm 1} \{\varepsilon^2 + u(x + \sqrt{2}\varepsilon b v)\} \tag{3.2}$$

$$= \min_{||v||=1} \max_{b=\pm 1} \{\varepsilon^2 + u(x) + \sqrt{2}\varepsilon b v \cdot \nabla u(x) + \varepsilon^2 v^T \cdot D^2 u \cdot v + O(\varepsilon^3)\}. \tag{3.3}$$

In the latter step we expanded $u(x + \sqrt{2}\varepsilon b v)$ by its Taylor series about x. Dividing by ε^2, cancelling $u(x)$, and noting that Carol will choose b to maximize the quantity inside the bracket, we have

$$0 = 1 + \min_{||v||=1} \{\frac{1}{\varepsilon}\sqrt{2}|v \cdot \nabla u(x)| + v^T \cdot D^2 u \cdot v + O(\varepsilon)\}. \tag{3.4}$$

Taking $\varepsilon \to 0$, we see that Paul is forced to choose v such that the first term in the min is zero, ie. $v = \pm \nabla^\perp u / |\nabla u|$ (the sign of v does not matter since the second term is quadratic in v). With our choice of v, using the observation (1.19), we arrive at

$$0 = 1 + \Delta_1 u(x), \tag{3.5}$$

with the boundary conditions $u = 0$ at $\partial\Omega$. The resulting partial differential equation (3.5) is closely related to the original problem (1.1) – the level set $u = t$ is the curve evolved from

$\partial\Omega$ by (1.4) up to time t. Hence, the closed curves $\partial\Omega_i$ tend to mean curvature evolutions of $\partial\Omega$ as $\varepsilon \to 0$. However, since we are interested in evolving the entire embedding function by mean curvature, rather than just a single curve, we will not discuss it further.

3.2 Motion by Mean Curvature

To derive the partial differential equation (1.1), we consider the following *maximum maturity time game*:

Game 2. *Paul and Carol play with the same rules as Game 1, but now with a different goal. Paul now has an objective function $u_0(x)$ and a maturity time T - his goal is to minimize u_0 at the time of maturity. More precisely, if $y(\cdot)$ is the piecewise linear path taken by Paul as a function of time, his goal, starting at some position x and time t, is*

$$\min_{y(\cdot)} u_0(y(T)) \qquad y(\cdot) \text{ : possible paths taken by Paul.} \tag{3.6}$$

As before, Paul moves $\sqrt{2}\varepsilon$ at every time step of size ε^2.

Let the value function for this game be

$$u^\varepsilon(x,t) = \left\{ \min_{y(\cdot)} u_0(y(T)) : y(\cdot) \text{ path starting at } x \text{ and time } t \right\}. \tag{3.7}$$

Since the rules are the same as Game 1, u^ε satisfies a similar dynamic programming principle:

$$u^\varepsilon(x,t) = \min_{||v||=1} \max_{b=\pm 1} u^\varepsilon(x + \sqrt{2}\varepsilon b v, t + \varepsilon^2) \tag{3.8}$$

We proceed as before, taking the limit $\varepsilon \to 0$ and the Taylor series in two dimensions (again, $u := \lim_{\varepsilon \to 0} u^\varepsilon$):

$$u(x,t) \approx \min_{||v||=1} \max_{b=\pm 1} u(x + \sqrt{2}\varepsilon b v, t + \varepsilon^2) \tag{3.9}$$

$$= \min_{||v||=1} \max_{b=\pm 1} \{u(x,t) + \sqrt{2}\varepsilon b v \cdot \nabla u + \varepsilon^2 (u_t + v^T \cdot D^2 u \cdot v) + O(\varepsilon^3)\} \tag{3.10}$$

After canceling $u(x,t)$, dividing by ε^2 and treating the $\max_{b=\pm 1}$, we obtain

$$0 = \min_{||v||=1} \left\{ \frac{1}{\varepsilon}\sqrt{2}|v \cdot \nabla u| + u_t + v^T \cdot D^2 u \cdot v + O(\varepsilon) \right\}. \tag{3.11}$$

Since $\varepsilon \to 0$, Paul is again forced to have $v = \pm\nabla^{\perp}u/|\nabla u|$. The resulting partial differential equation is

$$\begin{cases} u_t + \Delta_1 u = 0 & \text{for } t < T \\ u = u_0 & \text{at } t = T \end{cases} . \tag{3.12}$$

The partial differential equation (3.12) is not quite (1.1), (1.3); it can be made so by a change of variables $\tau = T - t$:

$$\begin{cases} u_\tau = \Delta_1 u & \text{for } \tau > 0 \\ u = u_0 & \text{at } \tau = 0 \end{cases} . \tag{3.13}$$

3.3 Curvature Motion

We saw in the last subsection that Game 2, at least heuristically, converges to the motion by mean curvature partial differential equation (1.1) as $\varepsilon \to 0$. We will now see that a small change in Game 2 yields the "positive" and the "negative" mean curvature flow, i.e.,

$$u_t = \left(\nabla \cdot \frac{\nabla u}{|\nabla u|}\right)_+ |\nabla u| \qquad \text{and} \qquad u_t = \left(\nabla \cdot \frac{\nabla u}{|\nabla u|}\right)_- |\nabla u|, \tag{3.14}$$

where $(x)_+ = \max(x, 0)$ and $(x)_- = \min(x, 0)$. If we "add" the right hand sides of (3.14), then we get the motion by mean curvature partial differential equation (1.1). Of course, it does not make sense to "add" two differential games. However, we will see in Chapter 5 that such approach is useful for the interpretation of numerical schemes.

3.3.1 Negative Curvature Motion

We first present a modified version of Game 2.

Game 3. *Paul and Carol play with the same rules as Game 2, except that now he is allowed to travel, at each time step ε^2, any distance within $\sqrt{2}\varepsilon$. As before, Paul has an objective function $u_0(x)$ and a maturity time T - his goal is to minimize u_0 at the time of maturity.*

In other words, in Game 3, Paul may choose to move less than $\sqrt{2}\varepsilon$, should it be more advantageous for him.

When would this added flexibility prove profitable for Paul? If the level sets of u_0 are convex, Paul would always move in the tangent direction as much as possible to minimize his objective. Hence, the Game 2 and Game 3 are identical if the level sets of u_0 are convex.

Now, suppose a level set of u_0 is concave at some point, and Paul starts there. Then, by moving a distance $\sqrt{2}\varepsilon$, he is forced to move to where the objective u_0 is higher.

Now consider Game 3. Since Paul does not necessarily have to move at any time step, at a point where the level set is concave, he will choose not to move. Hence, from Paul's perspective of minimizing the objective, the rules of Game 3 are better than those of Game 2.

The dynamic programming principle applied to Game 3, using the same notation, yields the following:

$$u^\varepsilon(x,t) = \min_{||v||\leq 1} \max_{b=\pm 1} u^\varepsilon(x + \sqrt{2}\varepsilon b v, t + \varepsilon^2). \tag{3.15}$$

The same argument as before gives,

$$0 = \min_{||v||\leq 1} \left\{ \frac{1}{\varepsilon}\sqrt{2}|v \cdot \nabla u| + u_t + v^T \cdot D^2 u \cdot v + O(\varepsilon) \right\}. \tag{3.16}$$

The difference now is that v is parallel to $\nabla^\perp u/|\nabla u|$ (or just $\nabla^\perp u$) but not necessarily equal. Since we have the freedom to let $v = 0$, the minimization should give

$$\min_{||v||\leq 1, v\perp \nabla u} v^T \cdot D^2 u \cdot v = \left(\frac{\nabla^\perp u}{|\nabla u|}^T \cdot D^2 u \cdot \frac{\nabla^\perp u}{|\nabla u|} \right)_-. \tag{3.17}$$

The resulting partial differential equation for Game 3 is,

$$u_t + \left(\nabla \cdot \frac{\nabla u}{|\nabla u|} \right)_- |\nabla u| = 0, \tag{3.18}$$

for $t < T$, backwards in time. The change of variables $\tau := T - t$ gives

$$u_\tau = \left(\nabla \cdot \frac{\nabla u}{|\nabla u|} \right)_- |\nabla u| \tag{3.19}$$

$$= (\kappa)_- |\nabla u| \tag{3.20}$$

for $\tau > 0$, and $u = u_0$ at $\tau = 0$.

Hence, Game 3 yields the "negative" curvature motion.

3.3.2 Positive Curvature Motion

We consider what Kohn and Serfaty refer to in [14], as the "inverse game" of Game 3.

Game 4 (Inverse game). *Paul and Carol play with the same rules as Game 1, except that now the goal is exactly opposite: Paul's goal is to stay inside Ω as long as possible, while Carol wants to steer him out. Also, as in Game 3, Paul may move, at each time step, a distance up to and including $\sqrt{2}\varepsilon$.*

Note that this is not a time dependent problem; the formulation is similar to (3.1). The dynamic programming principle is now,

$$u^\varepsilon(x) = \max_{\|v\|\leq 1} \min_{b=\pm 1} \{\varepsilon^2 + u^\varepsilon(x + \sqrt{2}\varepsilon b v)\}. \tag{3.21}$$

Similar argument follows:

$$\begin{aligned}
0 &\approx \max_{\|v\|\leq 1} \min_{b=\pm 1} \left\{ \frac{1}{\varepsilon} b\sqrt{2} v \cdot \nabla u + v^T \cdot D^2 u \cdot v \right\} && (3.22)\\
&= \max_{\|v\|\leq 1} \left\{ -\frac{1}{\varepsilon} |\sqrt{2} v \cdot \nabla u| + v^T \cdot D^2 u \cdot v \right\} && (3.23)\\
&= \max_{\|v\|\leq 1, v\perp \nabla u} \left\{ v^T \cdot D^2 u \cdot v \right\} && (3.24)\\
&= \left(\frac{\nabla^\perp u}{|\nabla u|}^T \cdot D^2 u \cdot \frac{\nabla^\perp u}{|\nabla u|} \right)_+ && (3.25)\\
&= \left(\nabla \cdot \frac{\nabla u}{|\nabla u|} \right)_+ |\nabla u|. && (3.26)
\end{aligned}$$

Finally, we derive the time dependent form of the partial differential equation. We present the inverse game with the objective function.

Game 5 (Time dependent inverse game). *Paul and Carol play with the same rules as Game 3, except that now the goal is exactly opposite: Paul's goal is to move such as to maximize the given objective function u_0, while Carol tries to obstruct him. Also, as in Game 3, Paul may move, at each time step of size ε^2, a distance up to and including $\sqrt{2}\varepsilon$.*

The now familiar dynamic programming principle for Game 5 becomes,

$$u^\varepsilon(x,t) = \max_{\|v\|\leq 1} \min_{b=\pm 1} u^\varepsilon(x + \sqrt{2}\varepsilon b v, t + \varepsilon^2), \tag{3.27}$$

and the heuristic derivation of the corresponding partial differential equation becomes,

$$
\begin{aligned}
0 &\approx \max_{||v||\leq 1} \min_{b=\pm 1} \left\{ \frac{1}{\varepsilon} b\sqrt{2} v \cdot \nabla u + u_t + v^T \cdot D^2 u \cdot v \right\} && (3.28)\\
&= \max_{||v||\leq 1} \left\{ -\frac{1}{\varepsilon} |\sqrt{2} v \cdot \nabla u| + u_t + v^T \cdot D^2 u \cdot v \right\} && (3.29)\\
&= u_t + \max_{||v||\leq 1, v\perp \nabla u} \left\{ v^T \cdot D^2 u \cdot v \right\} && (3.30)\\
&= u_t + \left(\frac{\nabla^\perp u}{|\nabla u|}^T \cdot D^2 u \cdot \frac{\nabla^\perp u}{|\nabla u|} \right)_+ . && (3.31)
\end{aligned}
$$

The resulting partial differential equation for Game 5, after the change of variables $\tau := T - t$, is

$$
\begin{aligned}
u_\tau &= \left(\nabla \cdot \frac{\nabla u}{|\nabla u|} \right)_+ |\nabla u| && (3.32)\\
&= (\kappa)_+ |\nabla u|. && (3.33)
\end{aligned}
$$

for $\tau > 0$, and $u = u_0$ at $\tau = 0$.

Hence, Game 5 yields the "positive" curvature motion.

3.3.3 Remarks

We emphasize that, algebraically,

$$u_t = (\kappa)_+ |\nabla u| + (\kappa)_- |\nabla u|, \tag{3.34}$$

is equivalent to the motion by mean curvature partial differential equation (1.1) but from game interpretation perspective, it is meaningless. Numerical interpretations relating to (3.34) will be presented in Chapter 5.

We also note that for the negative curvature flow, the boundary of a closed set will evolve into its convex hull, as in Figure 3.2. This makes sense from the perspective of the game. If Paul is currently at a location where the level set is convex, then his strategy would be to not move – any move in the tangent direction will cause the objective function to increase.

3.4 Theorems

In deriving partial differential equations, we have only argued heuristically and formally. Rigorous proofs confirming these claims were shown by R. Kohn, S. Serfaty, G. Barles and

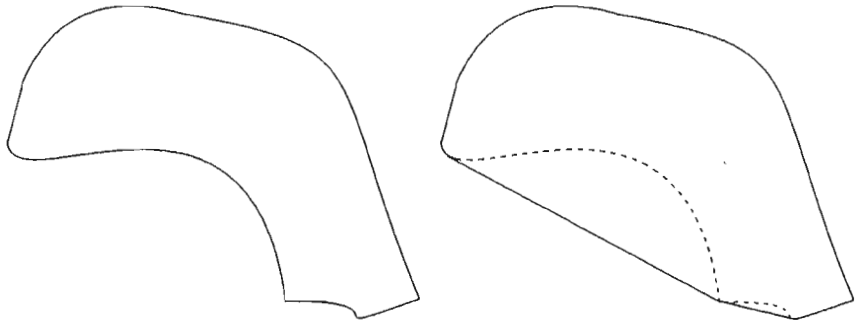

Figure 3.2: The convex hull. Left to right: initial curve; its convex hull (the dotted line shows a part of the initial curve).

F. Da Lio (the latter two authors contribute in the appendix) in [14]. We will present only the relevant theorems involving the games introduced in this section. In essence, the value functions for all the games converge to the unique viscosity solutions of the formally derived partial differential equations.

Theorem 3.4.1 (Convergence for Game 2, motion by mean curvature). *For Game 2, suppose the objective function u_0 is continuous. For some $\varepsilon > 0$, let $u^\varepsilon(x,t)$ be the associated value function. Then u^ε converges uniformly on compact sets to the unique viscosity solution of (3.12) as $\varepsilon \to 0$.*

Theorem 3.4.2 (Convergence for Game 3, negative curvature motion). *For Game 3, suppose the objective function u_0 is continuous. For some $\varepsilon > 0$, let $u^\varepsilon(x,t)$ be the associated value function. Then u^ε converges uniformly on compact sets to the unique viscosity solution of (3.19) as $\varepsilon \to 0$.*

Theorem 3.4.3 (Convergence for Game 5, positive curvature motion). *For Game 5, suppose the objective function u_0 is continuous. For some $\varepsilon > 0$, let $u^\varepsilon(x,t)$ be the associated value function. Then u^ε converges uniformly on compact sets to the unique viscosity solution of (3.32) as $\varepsilon \to 0$.*

For complete proofs, we refer the reader to [14].

Chapter 4

Numerical Analysis

Numerical schemes for motion by mean curvature have been well studied in several frameworks. Traditional, non-level set approaches, are surveyed in [23]. Finite element methods were studied in detail by Deckelnick, et al. [5].

We will only cover finite difference schemes, primarily due to their simplicity. In this chapter we present the necessary numerical analysis for understanding convergence of numerical schemes for degenerate elliptic partial differential equations. The bulk of this material is due to Oberman [19].

4.1 Preliminaries

4.1.1 Setup

Throughout this chapter, the setup will be as follows. A continuous function $u : [0,T] \times [-L_x, L_x] \times [-L_y, L_y] \to \mathbb{R}$ will be approximated on a uniform Cartesian grid of size $N_t \times N_x \times N_y$ by the *grid function* $u^n_{i,j}$, where $dt = T/(N_t - 1)$, $dx = 2L_x/(N_x - 1)$, $dy = 2L_y/(N_y - 1)$ and

$$u^n_{i,j} \approx u(n \cdot dt, i \cdot dx - L_x, j \cdot dy - L_y).$$

Points on the Cartesian grid will be referred to as *grid points* or *lattice points*. The arbitrary constants dt, dx and dy we shall call the *time step*, *grid spacing in* x and *grid spacing in* y, respectively. A *scheme* is a discrete function that maps a grid function to grid function. A *neighbourhood* of a scheme at a grid point (i,j) is the set of (local) grid points near (i,j),

denoted by $N(i,j)$, which influence the value at (i,j) at each time step. A *boundary point* is a grid point that has no neighbours[1]. For simplicity, if $u^n_{i,j}$ is the grid function of $u(x,y,t)$, we can describe a scheme $\mathcal{F}$ by the expression

$$\mathcal{F}[u] := \mathcal{F}\left(u_{i,j}, u_{i,j} - u_{\vec{k}}|_{\vec{k}\in N(i,j)}\right). \tag{4.1}$$

For conciseness, we may occasionally represent $(u_{i,j}, u_{i,j} - u_{\vec{k}}|_{\vec{k}\in N(i,j)})$ by $\xi \in \mathbb{R}^{|N(i,j)|+1}$, and denote the right hand side of (4.1) by $\mathcal{F}(\xi)$.

In some situations the *directional resolution* parameter, $d\theta$, is relevant. This parameter was first introduced in Oberman [19], [18] for schemes where $N(i,j)$ approximates points on a circle. The $d\theta$ is the maximum angle between two consecutive points in $N(i,j)$ that approximately lie on the circle with centre (i,j). For conciseness we denote the vector $d\vec{x} := [dx, dy, d\theta]$.

4.1.2 Consistency, Monotonicity and Stability

We define consistency for the Δ_1 operator in the sense of [18]. We must be careful as $\Delta_1 u$ does not exist in the classical sense where the gradient of u vanishes.

We denote schemes that are dependent on $d\vec{x}$ as $\mathcal{F}^{d\vec{x}}$ and schemes that further dependent on dt as $\mathcal{F}^{d\vec{x}}_{dt}$.

Definition 4.1.1 (Consistency for Δ_1). *The scheme $\mathcal{F}^{d\vec{x}}$ is* consistent *with $-\Delta_1$ if for every smooth function ϕ, and for every $x, y, t > 0$,*

$$\lim_{d\vec{x}\to 0} \mathcal{F}^{d\vec{x}}[\phi] = -\Delta_1 \phi \tag{4.2}$$

at (x,y,t) if $\nabla\phi \neq 0$, and

$$\lambda_{min} \leq \liminf_{d\vec{x}\to 0} \mathcal{F}^{d\vec{x}}[\phi] \leq \limsup_{d\vec{x}\to 0} \mathcal{F}^{d\vec{x}}[\phi] \leq \lambda_{max} \tag{4.3}$$

at (x,y,t) where $\lambda_{min}, \lambda_{max}$ are the minimum and maximum eigenvalues, respectively, of $-D^2\phi$, otherwise.

With a scheme $\mathcal{F}^{d\vec{x}}$ for the $-\Delta_1$ operator, the simplest scheme for the time dependent motion by mean curvature is the *explicit Euler map*:

$$S^{d\vec{x}}_{dt}[u] := u - dt\mathcal{F}^{d\vec{x}}[u]. \tag{4.4}$$

[1] Note that we will only be considering the Dirichlet problem of motion by mean curvature.

Intuitively, by updating $u_{i,j}^{n+1}$ by $(S_{dt}^{d\vec{x}}[u^n])_{i,j}$ at each time step and grid point (i,j), $u_{i,j}^n$ should approximate the solution to motion by mean curvature (1.1) as $d\vec{x}, dt \to 0$. In the rest of this chapter, we will present the relevant machinery and results that allow us to guarantee that such updating indeed solves (1.1).

We define two important properties of schemes: monotonicity and stability in the maximum norm. The norm $||\cdot||_{L^\infty}$ is the component-wise maximum norm.

Definition 4.1.2 (Monotonicity). *Given grid functions u and v, a scheme $\mathcal{F}$ is* monotone *if $u \leq v$ component-wise implies*

$$\mathcal{F}[u] \leq \mathcal{F}[v]. \tag{4.5}$$

Definition 4.1.3 (Stability in the maximum norm). *Given grid functions u and v, a scheme $\mathcal{F}$ is* stable in the maximum norm *if*

$$||\mathcal{F}[u] - \mathcal{F}[v]||_{L^\infty} \leq ||u - v||_{L^\infty}. \tag{4.6}$$

4.1.3 Theorem of Barles and Souganidis

The Lax Equivalence Theorem for initial value problems arising in conservation laws [12] requires two criteria for convergence: consistency and stability. For degenerate elliptic partial differential equations, there is a further extra criterion for convergence: monotonicity. The following fundamental result is due to Barles and Souganidis [1].

Theorem 4.1.4 (Barles and Souganidis, 1991). *Consider a degenerate elliptic partial differential equation for which there exist unique viscosity solutions. A consistent, stable approximation scheme converges to the unique viscosity solution provided it is monotone.*

Theorem 4.1.4 will be our guiding recipe for constructing finite difference schemes that converge to the unique viscosity solution of (1.1).

4.2 Degenerate Elliptic Schemes

In Chapter 2, we encountered the notion of degenerate elliptic partial differential equations, and showed that (2.1) is degenerate elliptic. Now we define *degenerate elliptic schemes.*

Definition 4.2.1 (Degenerate elliptic schemes). *Consider the scheme $\mathcal{F}$ as in (4.1). We call $\mathcal{F}$* degenerate elliptic *if each argument of $\mathcal{F}$ is nondecreasing in each variable, i.e.*

nondecreasing in $u_{i,j}$ *and in* $(u_{i,j} - u_{\bar{k}}|_{\bar{k}\in N(i,j)})$.
Furthermore, we call $\mathcal{F}$ degenerate elliptic with Lipschitz constant K *if there exists some constant* K *such that, for any* $\xi, \zeta \in \mathbb{R}^{|N(i,j)|+1}$ *and at all grid points* (i,j), *the following holds:*

$$|(\mathcal{F}(\xi))_{i,j} - (\mathcal{F}(\zeta))_{i,j}| \leq K||\xi - \zeta||_{L^\infty}, \tag{4.7}$$

where $(\mathcal{F}(\xi))_{i,j}$ *denotes the value of the grid function* $\mathcal{F}(\xi)$ *at the grid point* (i,j).

We saw in Chapter 2 that the definition of viscosity solutions for (1.1) followed naturally from the notion of degenerate elliptic partial differential equations. Likewise, properties such as existence, uniqueness, comparison principle and contraction all followed from the definition of viscosity solutions. We now see that the notion of degenerate elliptic schemes is linked with monotonicity and stability in the maximum norm for consistent explicit Euler maps. We emphasize that consistency, monotonicity and stability are sufficient for convergence to the unique viscosity solution of (1.1), due to Theorem 4.1.4.

Theorem 4.2.2 (Monotonicity and Stability of Euler Map). *Let* $\mathcal{F}^{d\bar{x}}$ *be a degenerate elliptic scheme with Lipschitz constant* K. *Then the corresponding explicit Euler map* $S_{dt}^{d\bar{x}}$ *as in (4.4) is monotone and stable in the maximum norm, provided*

$$dt \leq \frac{1}{K}. \tag{4.8}$$

Proof. We will only prove the monotonicity. For the proof on stability, see [19]. Let u and v be grid functions, and denote

$$\xi = (u_{i,j}, u_{i,j} - u_{\bar{k}}|_{\bar{k}\in N(i,j)}), \qquad \zeta = (v_{i,j}, v_{i,j} - v_{\bar{k}}|_{\bar{k}\in N(i,j)}) \tag{4.9}$$

Furthermore, assume that $u \leq v$, component-wise. It is sufficient to show that $S_{dt}^{d\bar{x}}[u] \leq S_{dt}^{d\bar{x}}[v]$.
First note that, due to the degenerate ellipticity (Definition 4.2.1) and Lipschitz continuity (4.7) of $\mathcal{F}^{d\bar{x}}$,

$$\begin{aligned} \mathcal{F}^{d\bar{x}}(\zeta) - \mathcal{F}^{d\bar{x}}(\xi) &\leq \mathcal{F}^{d\bar{x}}(\max\{\zeta,\xi\}) - \mathcal{F}^{d\bar{x}}(\xi) \\ &\leq K||\max\{\zeta,\xi\} - \xi||_{L^\infty} \\ &= K||\max\{\zeta - \xi, 0\}||_{L^\infty}, \end{aligned}$$

where $\max\{\cdot,\cdot\}$ is the componentwise maximum at each index. Furthermore, given (4.9), we have

$$\zeta - \xi = (v_{i,j} - u_{i,j}, (v_{i,j} - u_{i,j}) - (v_{\vec{k}} - u_{\vec{k}})|_{\vec{k}\in N(i,j)}).$$

But since $u \leq v$, we have that $(v_{\vec{k}} - u_{\vec{k}})|_{\vec{k}\in N(i,j)} \geq 0$, so

$$||\max\{\zeta - \xi, 0\}||_\infty \leq v_{i,j} - u_{i,j}$$

at each grid point (i,j).

Now, given the above results and the condition (4.8),

$$\begin{aligned} S_{dt}^{d\vec{x}}[u] - S_{dt}^{d\vec{x}}[v] &= u - v + dt(\mathcal{F}^{d\vec{x}}(\zeta) - \mathcal{F}^{d\vec{x}}(\xi)) \\ &\leq u - v + dt\ K||\max\{\zeta - \xi, 0\}||_{L^\infty} \\ &\leq u - v + dt\ K(v - u) \\ &= (1 - dt\ K)(u - v) \\ &\leq 0. \end{aligned}$$

□

We now have the sufficient set of tools to construct finite difference schemes for solving unique viscosity solutions to (1.1). For a function evolving according to the explicit Euler scheme (4.4) to converge to the unique viscosity solution of (1.1), the following properties are sufficient:

1. the scheme $\mathcal{F}$ is consistent with $-\Delta_1 u$,
2. $\mathcal{F}$ is degenerate elliptic with Lipschitz constant K, and
3. the time step dt satisfies $dt \leq 1/K$.

4.2.1 Remarks

When constructing numerical schemes, it is highly desirable that they obey properties characteristic of the underlying partial differential equation they model. For instance, the discrete maximum principle must be satisfied for approximating the heat equation [12], and likewise, the entropy condition for hyperbolic conservation laws [13].

In the case of motion by mean curvature, the counterpart is the comparison property, as outlined in Theorem 2.1.6. We mention here that the discrete version of the comparison

property, as well as the existence and uniqueness of the explicit Euler map follow from degenerate ellipticity and the Banach fixed point theorem. This line of argument is treated, with complete proofs, in [19].

4.3 Constructing Degenerate Elliptic Difference Schemes

In closing this chapter, we provide basic building blocks for constructing new degenerate elliptic schemes from known ones.

The key observation is due to Crandall, Ishii and Lions [4]: If $g : \mathbb{R}^k \to \mathbb{R}$ is a nondecreasing function of its arguments and $\mathcal{F}_i, i = 1, \ldots, k$ are degenerate elliptic schemes, then the scheme

$$\mathcal{F} = g(\mathcal{F}_1, \ldots, \mathcal{F}_k) \tag{4.10}$$

is degenerate elliptic. Futhermore, it is easy to see that the linear combination

$$\alpha_1 \mathcal{F}_1 + \alpha_2 \mathcal{F}_2 + \cdots + \alpha_k \mathcal{F}_k \tag{4.11}$$

is degenerate elliptic, provided $\alpha_i \geq 0$ for all $i = 1, \ldots, k$.

Some nondecreasing functions we will use to exploit the first property are the maximum, minimum and median functions, i.e.,

$$\begin{aligned} g(x_1, x_2, \ldots, x_k) &= \max\{x_1, x_2, \ldots, x_k\} \\ g(x_1, x_2, \ldots, x_k) &= \min\{x_1, x_2, \ldots, x_k\} \\ g(x_1, x_2, \ldots, x_k) &= \text{median}\{x_1, x_2, \ldots, x_k\}. \end{aligned}$$

It is also worth noting that $\mathcal{F} = 0$ is a degenerate elliptic scheme.

Chapter 5

Numerical Schemes

In this chapter, we present four schemes that numerically compute (1.1), or more precisely, evaluate the Δ_1 operator. Two of these will be nonmonotone and the other two monotone, in the sense of Definition 4.1.2. We will present provable convergence results for the monotone schemes, and remark on other issues such as stencil choice and boundary conditions.

We will also describe a link between the two monotone schemes for motion by mean curvature and the differential game interpretation of Chapter 3.

5.1 The Nonmonotone Schemes

The setup of the grid is as described in Section 4.1.1. We will also assume for simplicity that $dx = dy$. We present two schemes based on standard finite differences for solving (1.1) with some initial condition and Dirichlet boundary conditions. The initial data will be a grid function u^0, i.e. $u^0_{i,j} = u^0$. In presenting the schemes, only the iteration rule will be given.

We will use standard operator notation for forward, backward and centered differences:

$$\begin{aligned} D^+_x u_{i,j} &:= (u_{i+1,j} - u_{i,j})/dx \\ D^-_x u_{i,j} &:= (u_{i,j} - u_{i-1,j})/dx \\ D^0_x u_{i,j} &:= (u_{i+1,j} - u_{i-1,j})/(2dx) \\ D^2_x u_{i,j} &:= (u_{i+1,j} - 2u_{i,j} + u_{i-1,j})/dx^2 \end{aligned}$$

and similarly for $D^+_y, D^-_y, D^0_y, D^2_y$ in the y coordinate.

Scheme 1 (Centered Scheme). *Update by the rule*

$$\frac{u_{i,j}^{n+1}-u_{i,j}^{n}}{dt}=\frac{(D_y^0u_{i,j}^n)^2D_x^2u_{i,j}^n-2D_x^0u_{i,j}^nD_y^0u_{i,j}^nD_y^2(D_x^2u_{i,j}^n)+(D_x^0u_{i,j}^n)^2D_y^2u_{i,j}^n}{(D_x^0u_{i,j}^n)^2+(D_y^0u_{i,j}^n)^2}. \tag{5.1}$$

Scheme 2 (Divergence scheme). *Define*

$$\mathcal{D}_xu_{i,j}:=D_x^-\left[\frac{D_x^+u_{i,j}}{\sqrt{(D_x^+u_{i,j})^2+\frac{1}{2}(D_y^+u_{i+1/2,j})^2+\frac{1}{2}(D_y^-u_{i+1/2,j})^2}}\right] \tag{5.2}$$

and similarly for $\mathcal{D}_yu_{i,j}$. The value at the half-grid is the average of the two closest grid point values. Update by the rule

$$\frac{u_{i,j}^{n+1}-u_{i,j}^{n}}{dt}=\sqrt{\frac{(D_x^+u_{i,j}^n)^2+(D_x^-u_{i,j}^n)^2}{2}+\frac{(D_y^+u_{i,j}^n)^2+(D_y^-u_{i,j}^n)^2}{2}}\cdot(\mathcal{D}_xu_{i,j}^n+\mathcal{D}_yu_{i,j}^n). \tag{5.3}$$

We will refer to Scheme 1 as the *centered scheme*; the discretization follows from centre differencing all terms in (1.14). We will refer to Scheme 2 as the *divergence scheme* [15, Canonical scheme]; the discretization applies a forward-backward differencing on the divergence structure of (1.1). Both the centered and the divergence schemes are not monotone; hence, we will refer to these schemes as *nonmonotone schemes*. A standard elementary Taylor expansion argument shows that both schemes are consistent; we will not prove them here.

5.1.1 Drawbacks to the Nonmonotone Schemes

For a constant viscosity solution (Example 2.2.1), both nonmonotone schemes experience division by zeros. This can be overcome in at least two ways. One way is to modify the denominators of (5.1) and (5.2) by adding to them some $\varepsilon = O(dx^2)$. The error resulting in this modification is $O(dx^2)$. Another way is to call an if-then statement that sets the right hand sides of (5.1) and (5.3) to zero if their denominators are zero, i.e. the function there is nearly constant. This method exploits the fact that u in (1.1) is stationary in time wherever u is constant in space.

Aside from the aforementioned issue, nonmonotone schemes can cause undesirable diffusion for certain initial conditions. For more specific examples, see numerical examples in Section 6.2. There are no proofs to the author's knowledge that guarantee the convergence of nonmonotone schemes to the correct viscosity solution.

For practical purposes, another drawback for nonmonotone schemes is there are no known CFL-type conditions that guarantee their stability. For our numerical tests, the time step required to attain stability are chosen by trial and error to be $dt = dx^2/10$.

We also remark that both the centered and the divergence schemes are computationally intensive at each time step; this is a consequence of directly discretizing (1.1) by a usual finite difference approach.

5.2 The Median Scheme

The following scheme, called the *median scheme*, was proposed by Oberman [18].

Scheme 3 (Median scheme). *Let $N_m^n(i,j)$ denote a set of grid points that approximate a circle centred at (i,j) of radius $m \cdot dx$. Denote,*

$$u_{i,j}^{n*} = \text{median}\{u : u \in N_m^n(i,j)\}.$$

Update by the rule,

$$\frac{u_{i,j}^{n+1} - u_{i,j}^n}{dt} = 2\frac{u_{i,j}^{n*} - u_{i,j}^n}{(m \cdot dx)^2}. \tag{5.4}$$

We will clarify what we mean by approximating the circle in Section 5.2.1. We apply our recipe from Chapter 4 to check that the median scheme should indeed converge to the unique viscosity solution of (1.1). For this scheme, we read off the numerical operator for $-\Delta_1$ to be

$$\mathcal{F}_{med}^{d\vec{x}} = -2\frac{u_{i,j}^{n*} - u_{i,j}^n}{(m \cdot dx)^2}. \tag{5.5}$$

To see that $\mathcal{F}_{med}^{dx}$ is degenerate elliptic, we can write,

$$\mathcal{F}_{med}^{d\vec{x}} = \frac{2}{(m \cdot dx)^2}\text{median}_{\vec{k} \in N(i,j)}\left(u_{i,j}^n - u_{\vec{k}}^n\right), \tag{5.6}$$

where $N(i,j) := N_m^n(i,j)$. Since $\mathcal{F}_\alpha := u_{i,j}^n - u_{\vec{k}}^n$ is degenerate elliptic for $\vec{k} \in N(i,j)$, by (4.10) and (4.11), we have that $\mathcal{F}_{med}^{d\vec{x}}$ is also degenerate elliptic. Furthermore, note that for grid functions $u_{i,j}$ and $v_{i,j}$,

$$||\mathcal{F}_{med}^{d\vec{x}}(u)_{i,j} - \mathcal{F}_{med}^{d\vec{x}}(v)_{i,j}||_{L^\infty} = \frac{2}{(m \cdot dx)^2}||(u_{i,j} - u_{i,j}^*) - (v_{i,j} - v_{i,j}^*)||_{L^\infty}, \tag{5.7}$$

so $\mathcal{F}_{med}^{d\vec{x}}$ is degenerate elliptic with Lipschitz constant $2/(m \cdot dx)^2$. Consistency of the scheme,

$$2\frac{u_{i,j}^{n*} - u_{i,j}^n}{(m \cdot dx)^2} - \Delta_1 u = O(dx^2 + d\theta),$$

is proven in [18]. Hence, the explicit Euler scheme for $\mathcal{F}_{med}^{d\bar{x}}$ converges to the unique viscosity solution of (1.1) provided

$$dt \leq \frac{(m \cdot dx)^2}{2}. \tag{5.8}$$

We mention here a simple interpretation of why the median scheme solves (1.1). Observing (1.19), a scheme for the operator Δ_1 should mimic the one-dimensional heat equation

$$\frac{u_i^{n+1} - u_i^n}{dt} = \frac{u_{i+m}^n - 2u_i^n + u_{i-m}^n}{(m \cdot dx)^2}$$

in the direction of the tangent of the level curves of u. For sufficiently small dx, the median value of $N_m^n(i,j)$ is a reasonable approximation to u_{i+m}^n and u_{i-m}^n above. Hence, we arrive at (5.4).

5.2.1 Sample Stencils

We give sample *stencils* for the median scheme. By stencils, we are referring to the arrangement of $N(i,j) := N_m^n(i,j)$ with respect to (i,j). In practice, the stencil may be chosen to approximate a circle by hand. For our numerical results, we follow [18] and use the stencils shown in Figure 5.1. We will refer to them as level 0, 1, 2 and 3 stencils or schemes; their properties are outlined in Table 5.1.

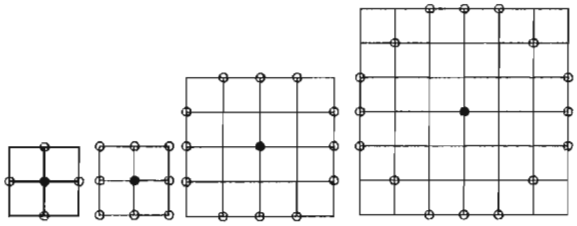

Figure 5.1: Stencils outlined in Table 5.1. The open circles denote the lattice points in $N(i,j)$. The grid spacing is dx, with the filled circle as the center point (i,j). Left to right: Level 0, 1, 2 and 3.

Interpolated Median Scheme

Note that the stencils in Figure 5.1 are circumscribed approximations to the circle of corresponding radii. For example, for the level 1 median scheme, wherever the level sets are nearly in the direction of $(1,1)$ or $(1,-1)$, the numerical solution propagates the level sets faster

Table 5.1: Median scheme stencil properties.

Level	# of neighbours	stencil radius	$d\theta$ directional resolution
0	4	dx	$\pi/2$
1	8	dx	$\pi/4$
2	12	$2dx$	$\pi/2 - 2\tan^{-1}(1/2)$
3	16	$3dx$	$\pi/4 - \tan^{-1}(1/3)$

than the exact solution. For wider stencils, the circumscribed approximations approach the circle, so the error in propagation decreases.

To obtain a better approximation for smaller stencils, we can linearly interpolate values on grid nodes onto the circle of corresponding radii. For example, the level 1 median scheme will still have eight neighbors, but the four "corners" will differ: for instance, the $u_{i+1,j+1}$ value in the original level 1 median scheme is replaced by $(\frac{1}{\sqrt{2}}u_{i+1,j+1} + \frac{\sqrt{2}-1}{\sqrt{2}}u_{i,j})$; see Figure 5.2.

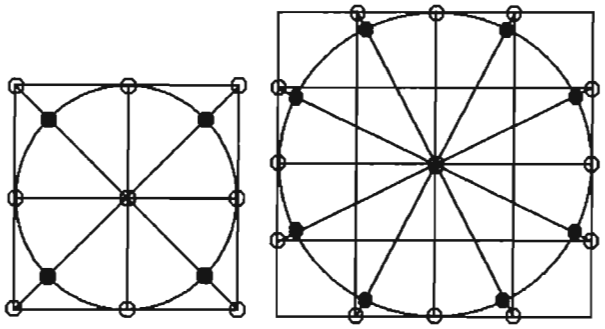

Figure 5.2: The interpolated median scheme stencils. Grid points that are not on the circle are interpolated onto the circle, shown by filled circles. Left to right: level 1 stencil; level 2 stencil.

The Median Scheme on a Hexagonal Grid

Another way to improve the circular approximation is to use a grid composed of equilateral triangles. The level 1 median scheme on such a grid will have six neighbors, all distance exactly dx from the center. We will call this the *hexagonal grid* from the shape of the level 1 stencil. As we will see in the next chapter, this stencil gives better accuracy than the level 1 median scheme on a Cartesian grid, despite having a larger $d\theta$. We note that the level 2 version of the median scheme on a hexagonal grid will not have neighbours of equal distance

from the center; hence, we will only consider the level 1 stencil.

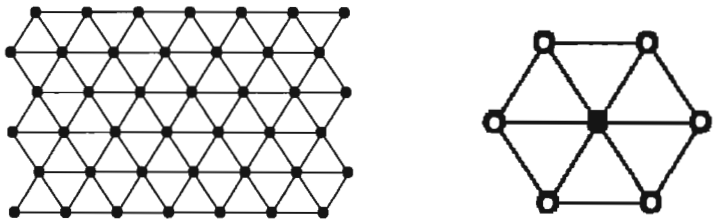

Figure 5.3: The median scheme on a hexagonal grid. Left to right: a hexagonal grid; the level 1 median scheme stencil on a hexagonal grid.

5.2.2 Boundary Conditions

Dirichlet boundary conditions are enforced by simply assigning values from the previous time step at the boundary points. For wider stencils, care must be taken in computing values near the boundary; the circle on which to compute the median must be deformed near the boundary to accommodate the wider stencil[1]. The deformed stencils are shown in Figure 5.4. For the interpolated median scheme, the interpolation can be computed only where the stencil is not deformed.

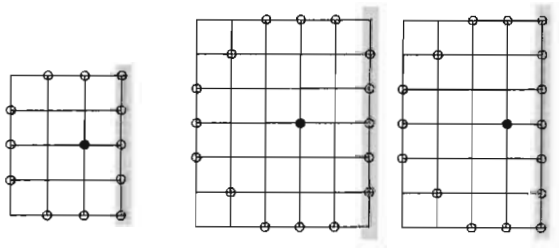

Figure 5.4: The median scheme near the boundary. Left to right: Level 2 stencil one lattice point from the boundary; Level 3 stencil two lattice points from the boundary; Level 3 stencil one lattice point from the boundary. The lattice points in the shaded boxes are the boundary points.

[1]As an exception, we employ simpler boundary conditions to better illustrate the point for the diagonal sine curve test in Sections 6.2 and 6.3. Since we know that straight level sets do not move, we enforce Dirichlet boundary conditions for all grid points $(m-1)$ pixel distances from the boundary for stencils of radius $m \cdot dx$.

5.2.3 Game Interpretation: The Median Scheme

We now establish a link between the median scheme and the differential game interpretation of Chapter 3.

Recall Game 2. To minimize the objective function u, Paul's strategy was to move in the tangent direction of the level set of u a distance $\sqrt{2}\varepsilon$, at each time step ε^2. As mentioned earlier, the median value on the boundary of a circular neighbourhood is a sensible approximation of the value in the tangent direction of the level set. Therefore, if

$$dt = \varepsilon^2 \text{ and } m \cdot dx = \sqrt{2}\varepsilon \text{ for some } \varepsilon > 0, \tag{5.9}$$

then

$$u_{i,j}^{n+1} = u_{i,j}^{n*}. \tag{5.10}$$

should be a scheme to solve (1.1). However, (5.9) is equivalent to having $dt = (m \cdot dx)^2/2$, which yields (5.10) when substituted into (5.4)! Thus, we have shown that (5.4) is a generalization of a discretization of Game 2.

5.3 The Morphological Scheme

The last scheme, the *morphological scheme*, is due to Catte, Dibos and Koepfler [2]. The name is derived from *morphological image processing*, a standard technique in digital filters [10].

Scheme 4 (Morphological scheme). *Denote $S_{h,\theta}(i,j)$ to be the set of grid points that are interpolated by a line with centre (i,j) of length (approximately) h and angle $\theta \in [0,\pi)$, and Θ to be some suitably chosen (finite, in practice) set of angles in $[0,\pi)$. Let m be a positive integer ($m \cdot dx$ is the stencil radius) and update by the rule,*

$$\frac{u_{i,j}^{n+1} - u_{i,j}^{n}}{dt} = \frac{1}{(m \cdot dx)^2} \left(\min_{\theta \in \Theta} \max_{\vec{k} \in S_{2m \cdot dx, \theta}(i,j)} (u_{\vec{k}}^n - u_{i,j}) + \max_{\theta \in \Theta} \min_{\vec{k} \in S_{2m \cdot dx, \theta}(i,j)} (u_{\vec{k}}^n - u_{i,j}) \right) \tag{5.11}$$

We check the degenerate ellipticity for the morphological scheme. The scheme for $-\Delta_1$ is

$$\mathcal{F}_{morph}^{d\vec{x}} = \frac{1}{(m \cdot dx)^2} \left(\min_{\theta \in \Theta} \max_{\vec{k} \in S_{2m \cdot dx, \theta}(i,j)} (u_{i,j} - u_{\vec{k}}^n) + \max_{\theta \in \Theta} \min_{\vec{k} \in S_{2m \cdot dx, \theta}(i,j)} (u_{i,j} - u_{\vec{k}}^n) \right). \tag{5.12}$$

Since $\mathcal{F}_\alpha := u^n_{i,j} - u^n_{\vec{k}}$ is degenerate elliptic for $\vec{k}$ in $N(i,j)$, taking the maximum and minimum (and vice versa), adding, and multiplying by $(m\ dx)^{-2}$ maintains its degenerate ellipticity. A similar argument to the median scheme imples that $\mathcal{F}^{d\vec{x}}_{morph}$ is degenerate elliptic with Lipschitz constant $2/(m \cdot dx)^2$.

The consistency of the morphological scheme in the sense of Definition 4.1.1 must be worked out. If u is smooth and $\nabla u \neq 0$, this turns out to be simple since the morphological scheme is identical to the median scheme when the stencils are chosen similarly (see Figure 5.7). To argue this, consider the median and the morphological scheme stencils with $d\theta = 0$, or, equivalently, $\Theta = [0, \pi)$. Then, the values to which the two schemes iterate the next time step when $dt = (m \cdot dx^2)/2$ is shown in Figure 5.5: each scheme outputs the average of the two squares. Note how, for $d\theta = 0$, the two schemes output different values. However, for some fixed $d\theta > 0$ and small enough stencil radius (in physical space), i.e. a finite m and small enough dx, the level sets are straight enough that both schemes output the same value; see Figure 5.6.

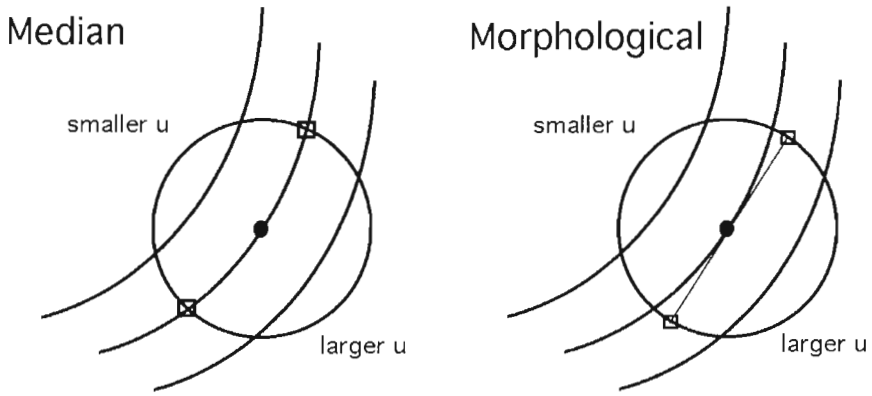

Figure 5.5: Schematic diagram of median and morphological scheme stencils where $\nabla u \neq 0$. The open-ended curves are the level sets of u, the circle is the stencil, and each scheme outputs the average of the two squares. Left to right: median scheme; morphological scheme.

Therefore,

$$-\frac{1}{(m\ dx)^2}\left(\min_{\theta\in\Theta}\max_{\vec{k}\in S_{2m\cdot dx,\theta}(i,j)}(u_{i,j}-u^n_{\vec{k}})+\max_{\theta\in\Theta}\min_{\vec{k}\in S_{2m\cdot dx,\theta}(i,j)}(u_{i,j}-u^n_{\vec{k}})\right)-\Delta_1 u = O(dx^2+d\theta).$$

However, at points where the gradient vanishes, the morphological scheme is *not* convergent in the sense of Definition 4.1.1. To describe the consistency behavior of the morphological

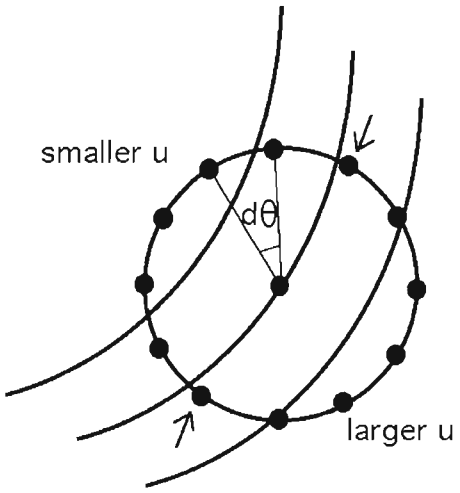

Figure 5.6: For a positive $d\theta$ and small enough stencil radius, the median and the morphological schemes (of the same stencil radius) output the average of the same two values, shown by the arrows. The black dots on the circle are the grid points that approximate the circle of the stencil radius.

scheme at singularities, we consider the quadratic:

$$u(x,y) = c + \lambda_1 \frac{x^2}{2} + \lambda_2 \frac{y^2}{2}.$$

where c is some constant. There is no loss of generality since any $u(x,y)$ such that $\nabla u = 0$ can be represented as above under some coordinate system. The two eigenvalues of D^2u are λ_1 and λ_2. To avoid confusion of signs, we will check consistency by testing to see if $-\mathcal{F}^{d\bar{x}}_{morph}$ is between the two eigenvalues of D^2u. Let the grid point (i,j) lie directly on the origin; i.e.

$$u_{i,j} = u(0,0) = c.$$

We classify the convergence behavior at the origin into three cases:

Case 1: $\lambda_1\lambda_2 \leq 0$

The origin is either a saddle point or, when one of the eigenvalues is zero, a non-strict (or degenerate) local extrema. Assume, without the loss of generality, that $\lambda_1 \leq 0 \leq \lambda_2$. Furthermore, assume that we are on a hypothetical grid where $d\theta = 0$, i.e. $\Theta = [0, \pi)$, an uncountably infinite set. The latter assumption lets us omit errors of $O(d\theta)$ in our analysis.

We check the consistency requirement of Definition 4.1.1.

For the term

$$\min_{\theta\in\Theta} \max_{\vec{k}\in S_{2m\cdot dx,\theta}(i,j)} (u_{\vec{k}} - u_{i,j})$$

the minimization over Θ implies $\theta = 0$, i.e. in the $(1,0)$ direction, the eigenvector of λ_1. Note that λ_1 is that smaller eigenvalue. This choice of θ minimizes the maximum of $u_{\vec{k}} - u_{i,j}$ along $S_{2m\cdot dx,\theta}(i,j)$. The maximum value of $u_{\vec{k}} - u_{i,j}$ along $S_{2m\cdot dx,0}(i,j)$ occurs at the origin, i.e. at $\vec{k} = (i,j)$, so

$$\min_{\theta\in\Theta} \max_{\vec{k}\in S_{2m\cdot dx,\theta}(i,j)} (u_{\vec{k}} - u_{i,j}) = 0 + c - c = 0.$$

Similarly, for the term

$$\max_{\theta\in\Theta} \min_{\vec{k}\in S_{2m\cdot dx,\theta}(i,j)} (u_{\vec{k}} - u_{i,j}),$$

the maximizing θ will be $\pi/2$, i.e. in the $(0,1)$ direction, the eigenvector of λ_2. The minimum value of $u_{\vec{k}} - u_{i,j}$ along $S_{2m\cdot dx,\pi/2}(i,j)$ occurs at the origin, i.e. $(x,y) = (0,0)$, or $\vec{k} = (i,j)$, so

$$\max_{\theta\in\Theta} \min_{\vec{k}\in S_{2m\cdot dx,\theta}(i,j)} (u_{\vec{k}} - u_{i,j}) = 0 + c - c = 0.$$

Combining these results, we have,

$$\begin{aligned} -\mathcal{F}^{d\vec{x}}_{morph} &= \frac{1}{(m\cdot dx)^2}\left(\min_{\theta\in\Theta} \max_{\vec{k}\in S_{2m\cdot dx,\theta}(i,j)} (u^n_{\vec{k}} - u_{i,j}) + \max_{\theta\in\Theta} \min_{\vec{k}\in S_{2m\cdot dx,\theta}(i,j)} (u^n_{\vec{k}} - u_{i,j})\right). \\ &= \frac{1}{(m\cdot dx)^2}(0+0). \\ &= 0 \in [\lambda_1, \lambda_2]. \end{aligned}$$

Hence, the morphological scheme is consistent with $\Delta_1 u$ according to Definition 4.1.1.

Case 2: $\lambda_1, \lambda_2 > 0$

The point is a (strict) local minimum. Assume, without the loss of generality, that $\lambda_1 \geq \lambda_2 > 0$. Furthermore, assume again that we are on a hypothetical grid where $d\theta = 0$.

We check the consistency requirement of Definition 4.1.1.

For the term

$$\min_{\theta\in\Theta} \max_{\vec{k}\in S_{2m\cdot dx,\theta}(i,j)} (u_{\vec{k}} - u_{i,j})$$

the minimization over Θ implies $\theta = \pi/2$, i.e. in the $(0,1)$ direction, the eigenvector of λ_2. Note that λ_2 is that smaller eigenvalue. This choice of θ minimizes the maximum of

$u_{\vec{k}} - u_{i,j}$ along $S_{2m\cdot dx,\theta}(i,j)$. The maximum value of $u_{\vec{k}} - u_{i,j}$ along $S_{2m\cdot dx,\pi/2}(i,j)$ occurs where $(x,y) = (0, m\cdot dx)$, or $\vec{k} = (i, j+m)$, so

$$\min_{\theta\in\Theta} \max_{\vec{k}\in S_{2m\cdot dx,\theta}(i,j)} (u_{\vec{k}} - u_{i,j}) = \lambda_2 \frac{(m\cdot dx)^2}{2} + c - c = \lambda_2 \frac{(m\cdot dx)^2}{2}.$$

Similarly, for the term

$$\max_{\theta\in\Theta} \min_{\vec{k}\in S_{2m\cdot dx,\theta}(i,j)} (u_{\vec{k}} - u_{i,j}),$$

the maximizing θ will be 0, i.e. in the $(1,0)$ direction, the eigenvector of λ_1. The minimum value of $u_{\vec{k}} - u_{i,j}$ along $S_{2m\cdot dx,0}(i,j)$ occurs at the origin, i.e. $(x,y) = (0,0)$, or $\vec{k} = (i,j)$, so

$$\max_{\theta\in\Theta} \min_{\vec{k}\in S_{2m\cdot dx,\theta}(i,j)} (u_{\vec{k}} - u_{i,j}) = 0 + c - c = 0.$$

Combining these results, we have,

$$\begin{aligned} -\mathcal{F}^{d\vec{x}}_{morph} &= \frac{1}{(m\cdot dx)^2}\left(\min_{\theta\in\Theta} \max_{\vec{k}\in S_{2m\cdot dx,\theta}(i,j)} (u^n_{\vec{k}} - u_{i,j}) + \max_{\theta\in\Theta} \min_{\vec{k}\in S_{2m\cdot dx,\theta}(i,j)} (u^n_{\vec{k}} - u_{i,j})\right). \\ &= \frac{1}{(m\cdot dx)^2}\left(\lambda_2 \frac{(m\cdot dx)^2}{2} + 0\right). \\ &= \frac{\lambda_2}{2} \notin [\lambda_2, \lambda_1]. \end{aligned}$$

Hence, the morphological scheme is inconsistent: $-\mathcal{F}^{d\vec{x}}_{morph}$ underestimates $\Delta_1 u$ according to Definition 4.1.1 by $\frac{\lambda_2}{2}$.

Case 3: $\lambda_1, \lambda_2 < 0$

The point is a (strict) local maximum. Assume again that $\lambda_1 \leq \lambda_2 < 0$. Furthermore, assume again that we are on a hypothetical grid where $d\theta = 0$.

By the same argument as in the last case, for the first term, we have that

$$\min_{\theta\in\Theta} \max_{\vec{k}\in S_{2m\cdot dx,\theta}(i,j)} (u_{\vec{k}} - u_{i,j}) = 0 + c - c = 0.$$

Here, $\theta = 0$. For the second term,

$$\max_{\theta\in\Theta} \min_{\vec{k}\in S_{2m\cdot dx,\theta}(i,j)} (u_{\vec{k}} - u_{i,j}) = \lambda_2 \frac{(m\cdot dx)^2}{2} + c - c = \lambda_2 \frac{(m\cdot dx)^2}{2}.$$

Here, $\theta = \pi/2$. Combining the terms, we have

$$\begin{aligned} -\mathcal{F}^{d\vec{x}}_{morph} &= \frac{1}{(m \cdot dx)^2}\left(\min_{\theta\in\Theta}\max_{\vec{k}\in S_{2m\cdot dx.\theta}(i,j)}(u^n_{\vec{k}} - u_{i,j}) + \max_{\theta\in\Theta}\min_{\vec{k}\in S_{2m\cdot dx.\theta}(i,j)}(u^n_{\vec{k}} - u_{i,j})\right). \\ &= \frac{1}{(m \cdot dx)^2}\left(\lambda_2\frac{(m \cdot dx)^2}{2} + 0\right). \\ &= \frac{\lambda_2}{2} \notin [\lambda_1, \lambda_2]. \end{aligned}$$

Hence, the morphological scheme is inconsistent: $-\mathcal{F}^{d\vec{x}}_{morph}$ overestimates $\Delta_1 u$ according to Definition 4.1.1 by $\frac{\lambda_2}{2}$.

We summarize the consistency behavior of the morphological scheme at singularities. Let λ_1 and λ_2 be the eigenvalues of D^2u. Then,

$$-\mathcal{F}^{d\vec{x}}_{morph} - \Delta_1 u = \begin{cases} O(dx^2 + d\theta) & \text{if } \nabla u \neq 0 \\ O(dx^2 + d\theta) & \text{if } \lambda_1\lambda_2 \leq 0 \\ -\frac{\lambda_2}{2} + O(d\theta) & \text{if } \lambda_1 \geq \lambda_2 > 0 \\ \frac{\lambda_2}{2} + O(d\theta) & \text{if } \lambda_1 \leq \lambda_2 < 0 \end{cases}. \tag{5.13}$$

In conclusion, by Theorem 4.1.4, the corresponding explicit Euler scheme converges to the unique viscosity solution of (1.1) only when the function has no local extrema, provided that

$$dt \leq (m \cdot dx)^2/2.$$

5.3.1 Sample Stencils

The choice of stencils for the morphological scheme is similar to that of the median scheme. We will again refer to them as Level 0, 1, 2 and 3 stencils. The stencils are outlined in Table 5.2 and shown in Figure 5.7[2]. As with the median scheme, due to the circumscribed approximation of the circle (or disc, in this case), propagation of curves will be faster than the exact solution.

5.3.2 Boundary Conditions

The morphological scheme, like the median scheme, must be deformed near the boundary. Stencils near the boundary for the morphological scheme are shown in Figure 5.8. As for

[2] As with the median scheme, we employ thicker boundary conditions in Sections 6.2 and 6.3.

Table 5.2: Morphological scheme stencil properties.

Level	# of neighbours	# of directions $= \lvert\Theta\rvert$	stencil radius	$d\theta$ directional resolution
0	5	2	dx	$\pi/2$
1	9	4	dx	$\pi/4$
2	17	6	$2dx$	$\pi/2 - 2\tan^{-1}(1/2)$
3	29	8	$3dx$	$\pi/4 - \tan^{-1}(1/3)$

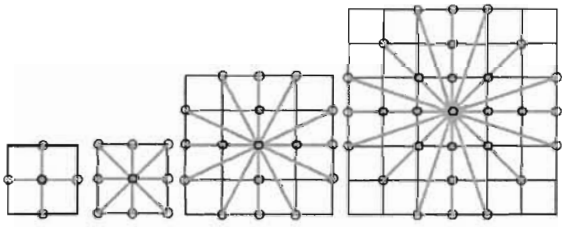

Figure 5.7: The morphological scheme stencils. The grid spacing is dx. The gray lines show the different directions Θ and the open black circles show the grid points that extrapolate them. Left to right: Level 0, 1, 2 and 3.

the median scheme, thicker boundary conditions will be used for numerical tests in Sections 6.2 and 6.3.

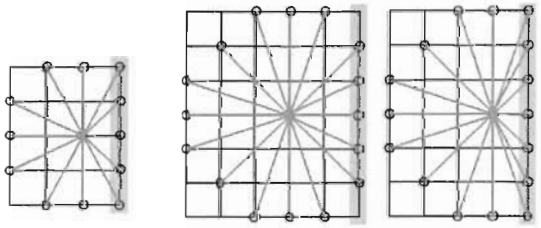

Figure 5.8: The morphological scheme near the boundary. Left to right: level 2 stencil one lattice point from the boundary; level 3 stencil two lattice points from the boundary; level 3 stencil one lattice point from the boundary. The lattice points in the shaded boxes are the boundary points.

5.3.3 Game Interpretation: the Morphological Scheme

Recall Game 3. If Paul has the choice of traveling a distance of *at most* $\sqrt{2}\varepsilon$, we showed that the resulting partial differential equation is the negative curvature flow (3.20). A reasonable way to discretize Paul's strategy is to evaluate the maximum of the minima along all possible

directions $\{S_{2\sqrt{2}\varepsilon,\theta}(i,j) : \theta \in \Theta\}$ at each time step and iterate:

$$u_{i,j}^{n+1} = \max_{\theta\in\Theta} \min_{\vec{k}\in S_{2\sqrt{2}\varepsilon,\theta}(i,j)} (u_{\vec{k}}^n), \tag{5.14}$$

where $dt = \varepsilon^2$. The justification for (5.14) is summarized:

> Paul knows that if he chooses v such that it points in a direction not tangent to the level set, Carol will reverse or not reverse v to his disadvantage. If Paul chooses a direction θ where the minimum of $S_{2\sqrt{2}\varepsilon,\theta}$ is not maximized, then θ is not pointing in the tangent direction and Carol will choose $b = \pm 1$ that puts him at a disadvantage.

Note that (5.14) will yield the same value as the median scheme where u is concave, and will be stationary where convex.

Repeating the argument for Game 5, a reasonable discretization of the positive curvature flow is

$$u_{i,j}^{n+1} = \min_{\theta\in\Theta} \max_{\vec{k}\in S_{2\sqrt{2}\varepsilon,\theta}(i,j)} (u_{\vec{k}}^n), \tag{5.15}$$

again where $dt = \varepsilon^2$. Note that (5.15) will yield the same value as the median scheme where u is convex, and will be stationary where concave.

By adding the equations (5.14) and (5.15) as described in (3.34), one has a discretization for (1.1):

$$u_{i,j}^{n+1} = \frac{1}{2}\left(\min_{\theta\in\Theta} \max_{\vec{k}\in S_{2\sqrt{2}\varepsilon,\theta}(i,j)} (u_{\vec{k}}^n) + \max_{\theta\in\Theta} \min_{\vec{k}\in S_{2\sqrt{2}\varepsilon,\theta}(i,j)} (u_{\vec{k}}^n)\right). \tag{5.16}$$

Since $m \cdot dx = \sqrt{2}\varepsilon$ and $dt = \varepsilon^2$, again we have that $dt = (m \cdot dx)^2/2$. Substituting this into (5.11) gives (5.16). Hence, we have shown that (5.11) is a generalization of a discretization of Games 3 and 5.

Insufficient diffusion

Recall that the consistency of the morphological scheme does not hold true at strict local extrema. We explore this in the game interpretation. For Game 3, Paul will choose not to move at a local minimum, while for Game 5, Paul will choose to move in any direction as much as possible. This is reflected by:

$$\max_{\theta\in\Theta} \min_{\vec{k}\in S_{2\sqrt{2}\varepsilon,\theta}(i,j)} (u_{\vec{k}}^n) = u_{i,j} \qquad \text{and} \qquad \min_{\theta\in\Theta} \max_{\vec{k}\in S_{2\sqrt{2}\varepsilon,\theta}(i,j)} (u_{\vec{k}}^n) = \max_{\vec{k}\in N_m(i,j)} u_{\vec{k}},$$

where $N_m(i,j)$ are lattice points approximately $m \cdot dx$ distance from (i,j). From the game interpretation, the updated value $u_{i,j}^{n+1}$ should be $\max_{\vec{k} \in N_m(i,j)} u_{\vec{k}}$. But by (5.16), this value would be halved. Hence, the change at the minimum for the morphological scheme is half of that in the exact solution. We will call this discrepancy *insufficient diffusion*. Insufficient diffusion is a direct consequence of the consistency failure of the morphological scheme at the strict local extrema.

From hereon, we will refer to the median and morphological schemes as *monotone schemes*.

Chapter 6

Numerical Experiments

In this section, we present various numerical experiments on artificial examples for the four schemes presented in the last chapter.

6.1 A Steady State Example

Before embarking on solving the time dependent problem (1.1), we test our schemes on the related steady state problem

$$0 = \Delta_1 u - 1. \tag{6.1}$$

The equation (6.1) is nearly identical to (3.5), except for an arbitrary chosen sign. This test reveals the characteristics of the scheme more clearly, as we need not consider numerical artifacts arising from time stepping. To solve (6.1), we numerically solve by the Euler method,

$$u_t = \Delta_1 u - 1 \tag{6.2}$$

until steady state.

The test is to run with initial condition

$$u_0(x, y) = \frac{1}{2}(x^2 + y^2)$$

which is already the steady state solution to (6.2). The domain is $[-1, 1]^2$. We measure the error between the exact solution u_0 and the numerical steady state solution.

6.1.1 The Median Scheme

The results of using the median scheme are shown in Figure 6.1. The level sets of the numerical solution approach those of the exact solution and their differences decrease as the stencils become wider. The numerical solution overestimates the exact solution in the interior since the stencils are circumscribed approximations of circles.

The level 1 and 2 interpolated median scheme results are shown in Figure 6.2. Note how the interpolated scheme has errors nearly half of those of the regular median scheme.

The results for the level 1 median scheme on a hexagonal grid are shown in Figure 6.3. Note how the results are about ten times better than the level 1 interpolated and non-interpolated median schemes, despite the fact that $d\theta$ is larger.

6.1.2 The Morphological Scheme

The results of using the morphological scheme are shown in Figure 6.4. For levels 1 and 2, the results resemble those of the median scheme in 6.1. However, for the level 3 stencil, the numerical solution underestimates the exact solution. This is due to insufficient diffusion, a phenomenon that grows as the stencil width widens. For wider stencils or sharper paraboloids, we expect the insufficient diffusion to grow – a weakness of the morphological scheme.

6.1.3 The Nonmonotone Schemes

The results of the centered and the divergence schemes are shown in Figure 6.5 and 6.6, respectively. The centered scheme solves to machine epsilon. The divergence scheme has an error of order 10^{-4} at the local minimum. This shows that the averaged forward-backward differencing is prone to lower accuracy than centered differencing at local extrema. Nevertheless, the nonmonotone schemes outperform the monotone schemes, despite the smaller stencils.

6.2 Diagonal Sine Curve

The initial condition to be tested is,

$$u_0(x, y) = u(x, y, 0) = \sin(4\pi(x - y))$$

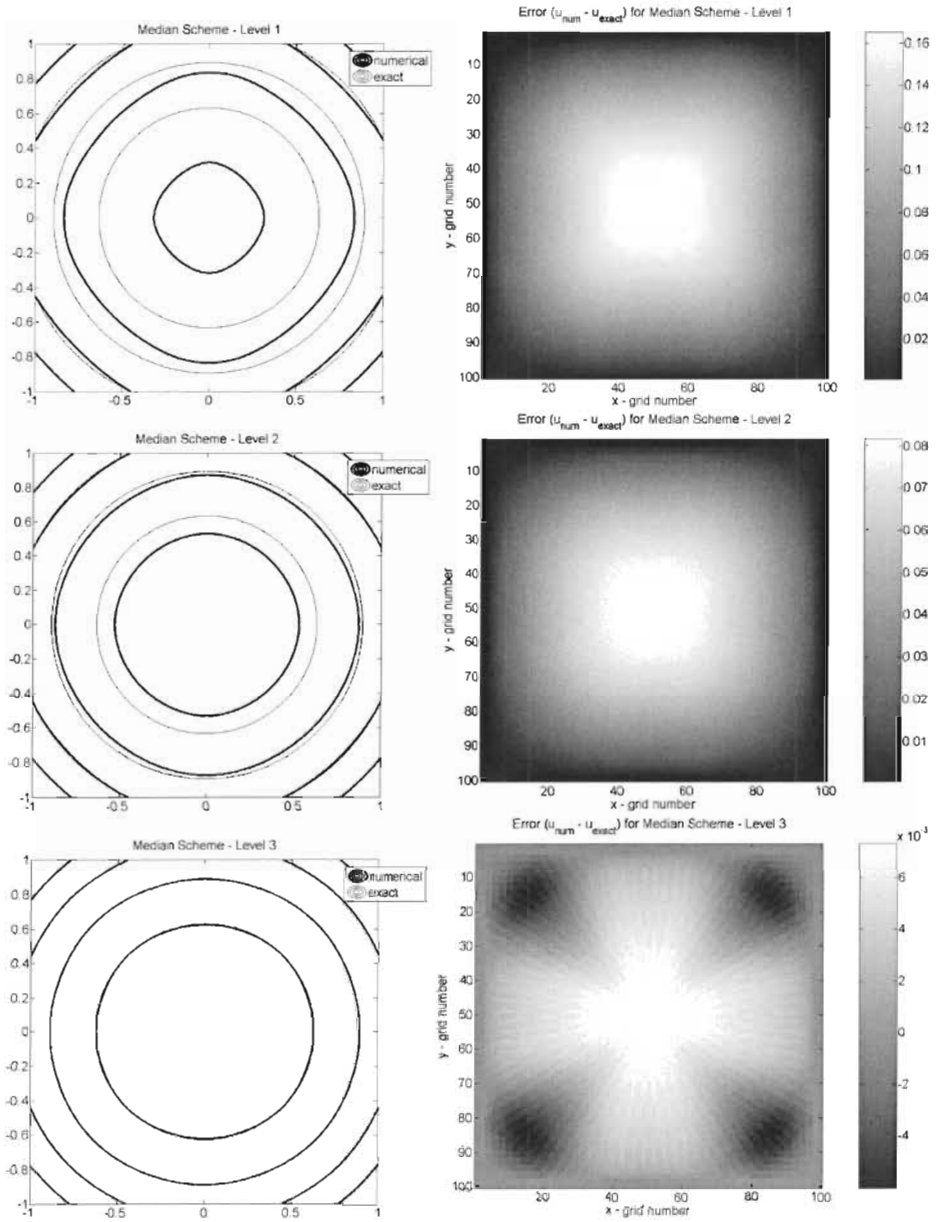

Figure 6.1: Steady state test for the median scheme. Sample level sets and the difference between the numerical and exact solution are shown. Top to bottom: level 1; level 2; level 3. Computations were performed on a 100^2 grid.

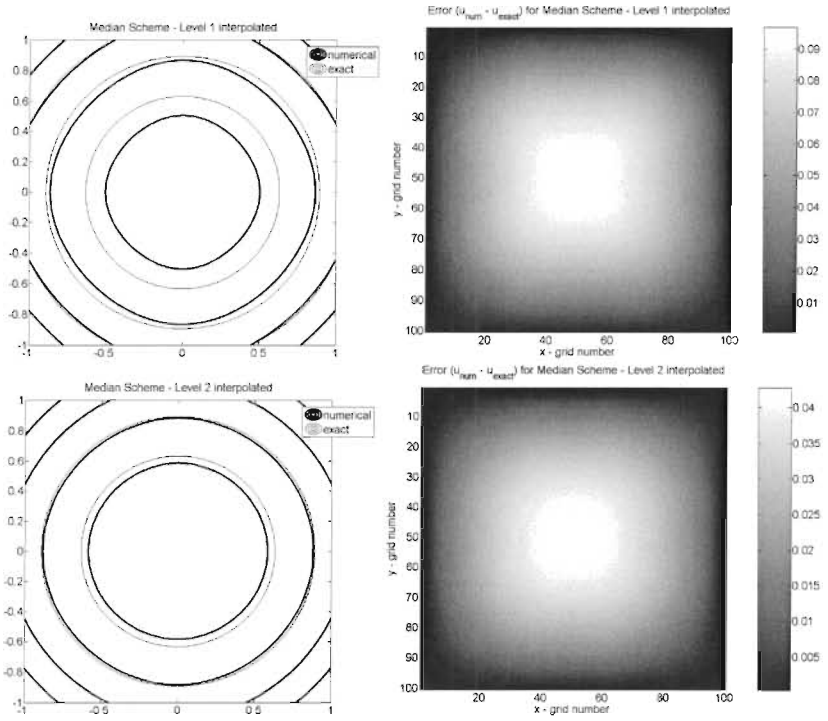

Figure 6.2: Steady state test for the interpolated median scheme. Sample level sets and the difference between the numerical and exact solution are shown. Top to bottom: level 1; level 2. Computations were performed on a 100^2 grid.

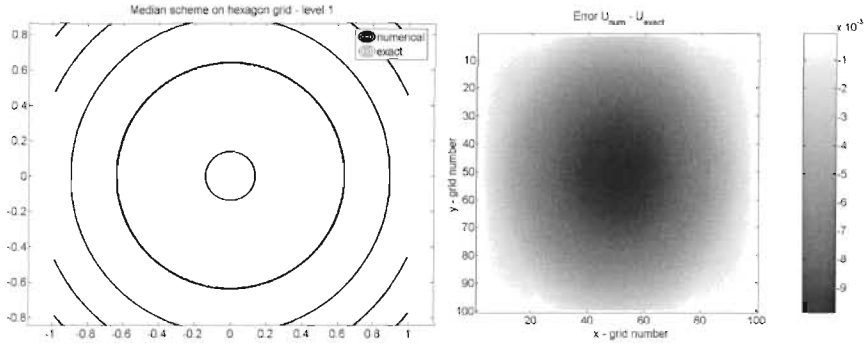

Figure 6.3: Steady state test for the level 1 median scheme on a hexagonal grid. Sample level sets and the difference between the numerical and exact solution are shown. Computations were performed on a 100^2 grid.

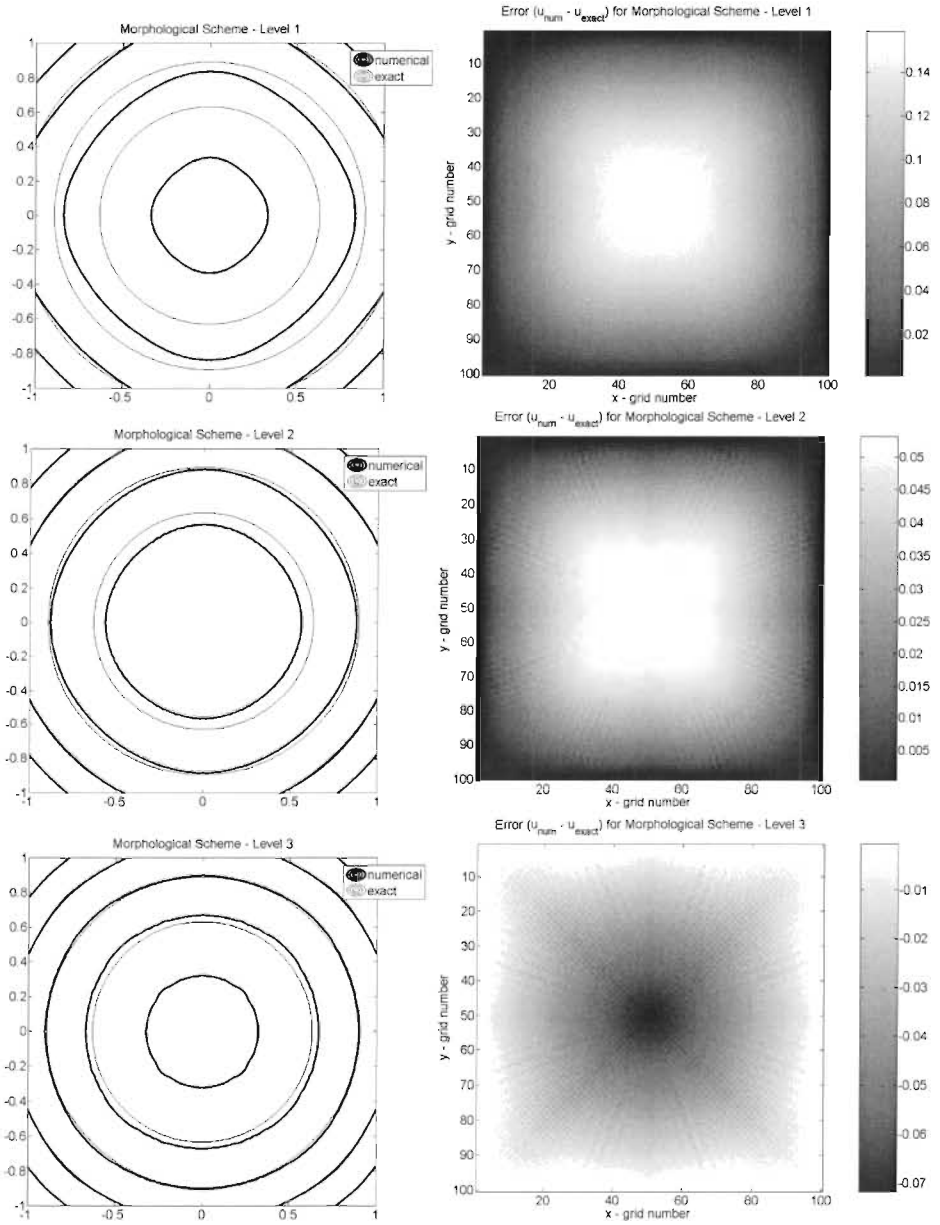

Figure 6.4: Steady state test for the morphological scheme. Sample level sets and the difference between the numerical and exact solution are shown. Top to bottom: level 1; level 2; level 3. Computations were performed on a 100^2 grid.

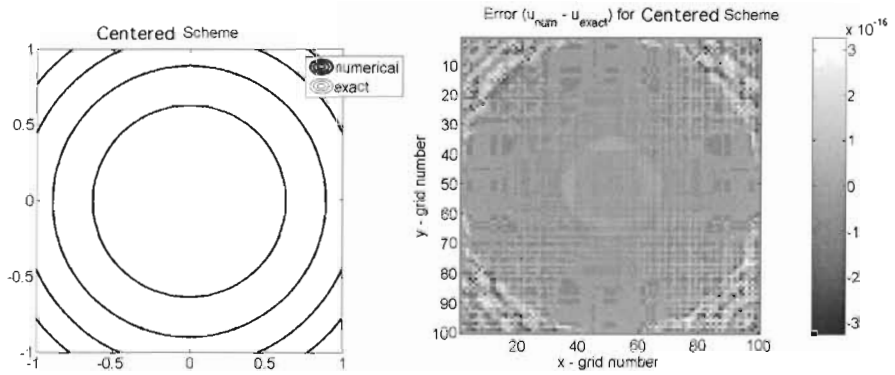

Figure 6.5: Steady state test for the centered scheme. Sample level sets and the difference between the numerical and exact solution are shown. Computations were performed on a 100^2 grid.

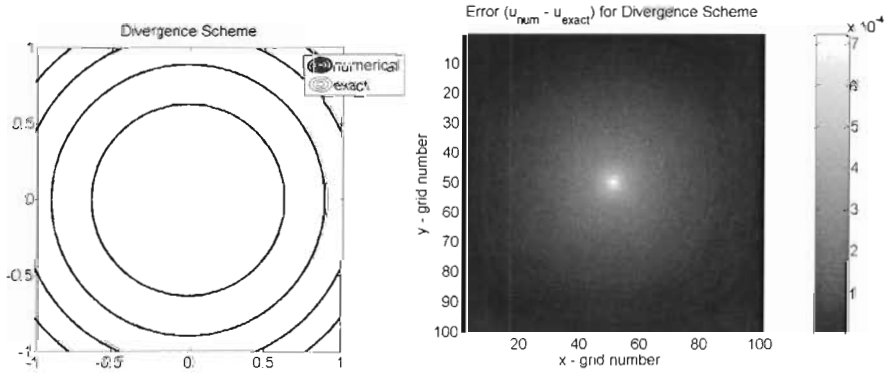

Figure 6.6: Steady state test for the divergence scheme. Sample level sets and the difference between the numerical and exact solution are shown. Computations were performed on a 100^2 grid.

in the domain $[0,1]^2$. Since u_0 has straight level sets, the solution of (1.1) should be stationary for $t > 0$.

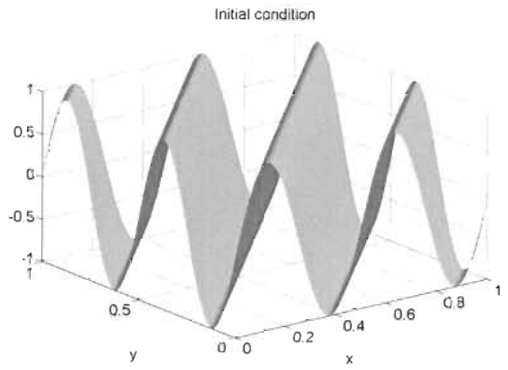

Figure 6.7: The initial condition u_0 for the diagonal sine curve test.

6.2.1 Median Scheme and Capping

For the level 1 median scheme, numerical diffusion of $O(dx^2)$ appears at the maxima and the minima. The width of this numerical diffusion is $2dx$. See Figure 6.9. In general, a stencil of radius $m \cdot dx$ would have a numerical diffusion of radius $2m \cdot dx$. We shall refer to this phenomenon as *capping*. For a schematic drawing of capping, see Figure 6.8. We emphasize that capping is finite numerical diffusion in that it occurs only for small finite time. In practice, if the stencil width is $m \cdot dx$, it usually takes m iterations for the capping to complete.

Capping for the median scheme can be explained from observing the scheme. At a maximum (or a minimum) of u, the median value of its neighbours would be less (or greater) than at the center. This causes the initial diffusion. More generally, any extremum along a linear manifold in a neighbourhood of radius $m \cdot dx$ experiences such diffusion. The diffusion thus stops when the width of the plateau, or capping, is $2m \cdot dx$.

We note that the max-norm error due to capping depends on the solution. The sine curve is nearly parabolic at its extrema, hence its capping of height $O(dx^2)$. For a sharper extremum, such as $|x|$ or $\sqrt{|x|}$, the error due to capping would be $O(dx)$ and $O(\sqrt{dx})$, respectively. The $O(dx^2)$ error due to capping for the diagonal sine curve example is confirmed in Figure 6.10.

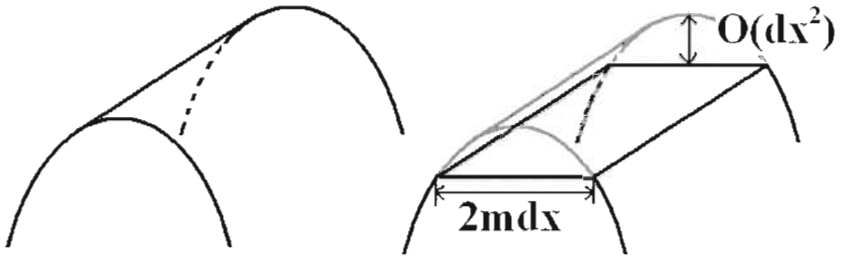

Figure 6.8: Schematic diagram of capping at a maximum of a sine curve. Left to right: initial condition; steady state solution (the initial condition is shown in gray).

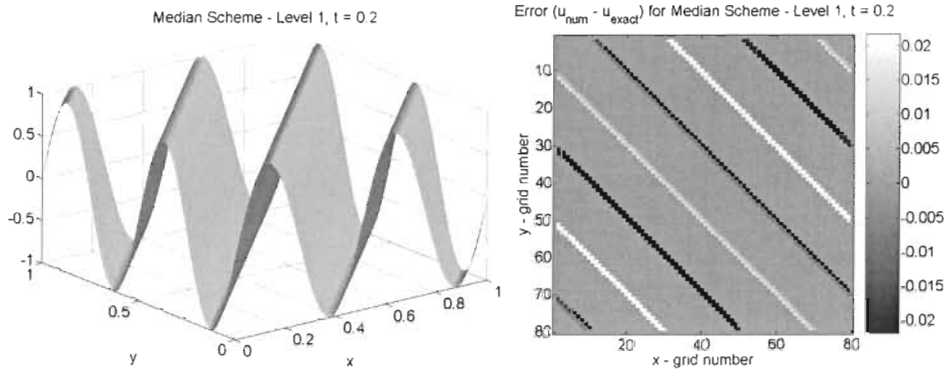

Figure 6.9: The level 1 median scheme result of the diagonal sine curve at $t = 0.2$. Left to right: numerical solution; the error to the exact solution. Computations were performed on a 80^2 grid.

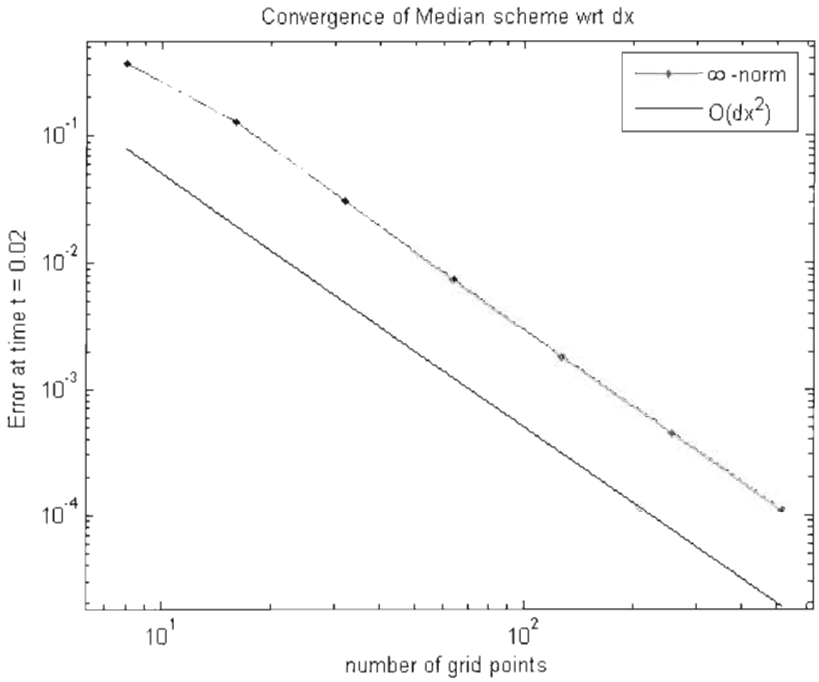

Figure 6.10: A plot of $O(dx^2)$ convergence for the level 1 median scheme for the diagonal sine curve example. The error is primarily due to capping.

6.2.2 Morphological Scheme

In theory, the morphological scheme should converge to the exact viscosity solution, since there are no strict local extrema. In fact, the morphological scheme gives the correct solution to machine epsilon; see Figure 6.11.

We mentioned earlier that the morphological scheme is identical to the median scheme where the function is smooth and has nonzero gradient. At saddle points and non-strict extrema, the morphological scheme does not induce capping like the median scheme. The min-max and the max-min operators of the morphological scheme correctly compute $\Delta_1 u$ to be zero. In this sense, the morphological scheme is superior to the median scheme.

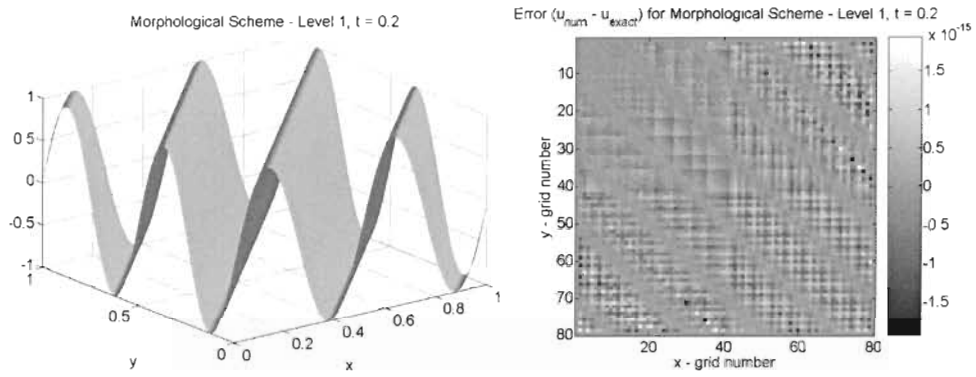

Figure 6.11: The level 1 morphological scheme result of the diagonal sine curve at $t = 0.2$. Left to right: numerical solution; the error to the exact solution. Computations were performed on a 80^2 grid.

6.2.3 Nonmonotone Schemes

Both the centered and divergence structure schemes diffuse excessively at the saddle points. They differ from capping in that the diffusion continues until errors are comparable to the initial data. See Figure 6.12 and 6.13 for results of the centered and the divergence schemes, respectively.

The excessive diffusion resulting for the divergence scheme can be explained geometrically. The divergence scheme essentially discretizes the divergence structure of (1.1), where $|\nabla u| = \sqrt{u_x^2 + u_y^2}$ is discretized by mixed forward and backward differences. Such discretization results in $|\nabla u| > 0$ at the saddle points. The discretization of $\nabla \cdot (\nabla u/|\nabla u|)$ also yields low accuracy: as shown in Figure 6.14, a discretization of $\nabla \cdot (\nabla u/|\nabla u|)$ would be negative

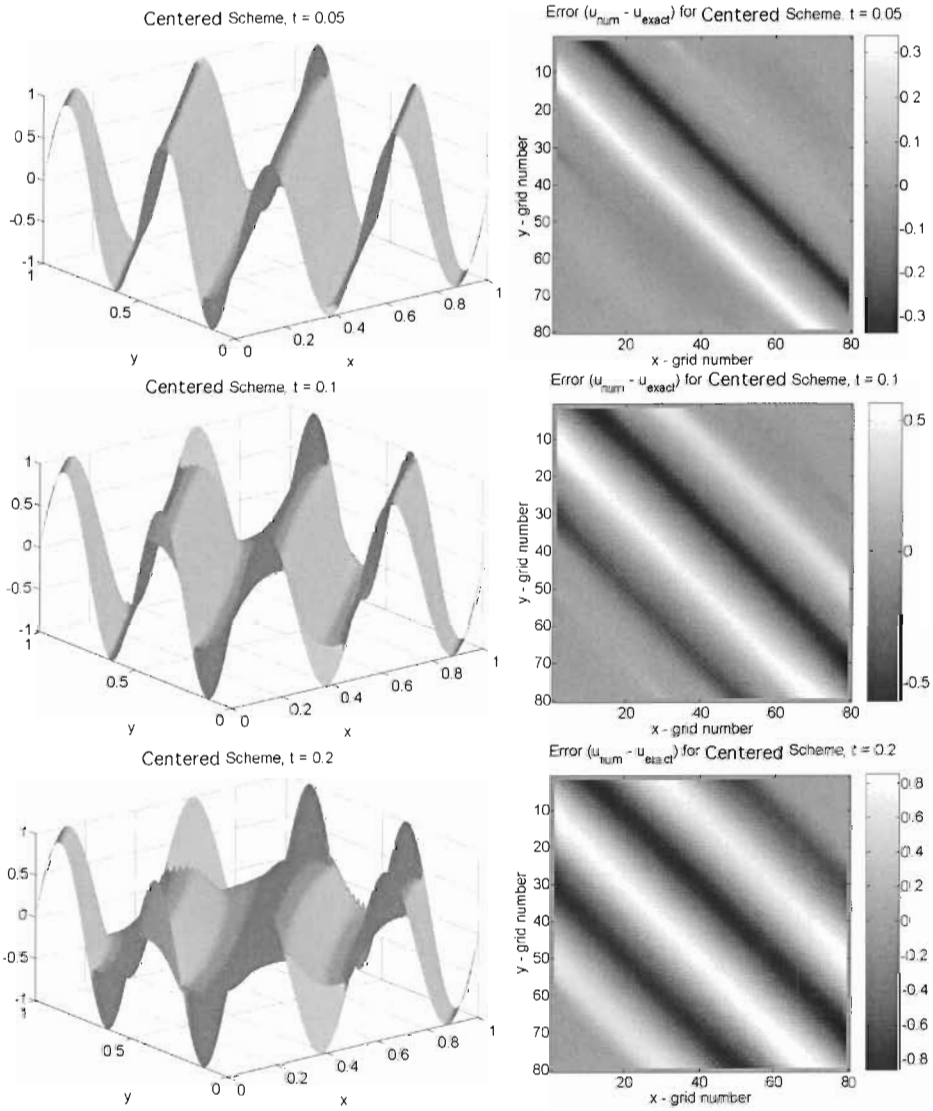

Figure 6.12: The solution by the centered scheme at $t = 0.05, 0.1, 0.2$. Computations were performed on a 80^2 grid.

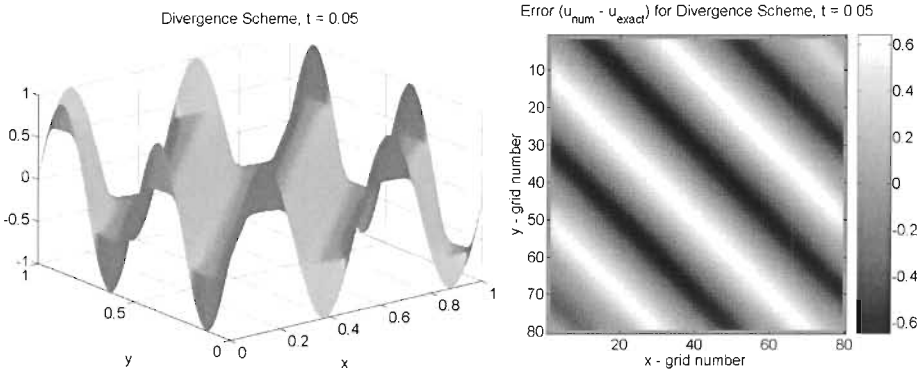

Figure 6.13: The solution by the divergence scheme at $t = 0.05$. Computations were performed on a 80^2 grid.

at the maxima (and positive at minima). Therefore, the divergence scheme will compute $\Delta_1 u$ to be negative at the maxima and positive at the minima - this is the cause of the diffusion. The fact that diffusion also occurs for the centered scheme may be explained by a similar argument. Although centered differences do compute u_x, u_y to be zero (to machine epsilon) at the extrema, the division in the denominator in (5.1) by a discretization of $|\nabla u|$, may amplify the non-zero nature of the right hand side. For larger grid spacing dx, the

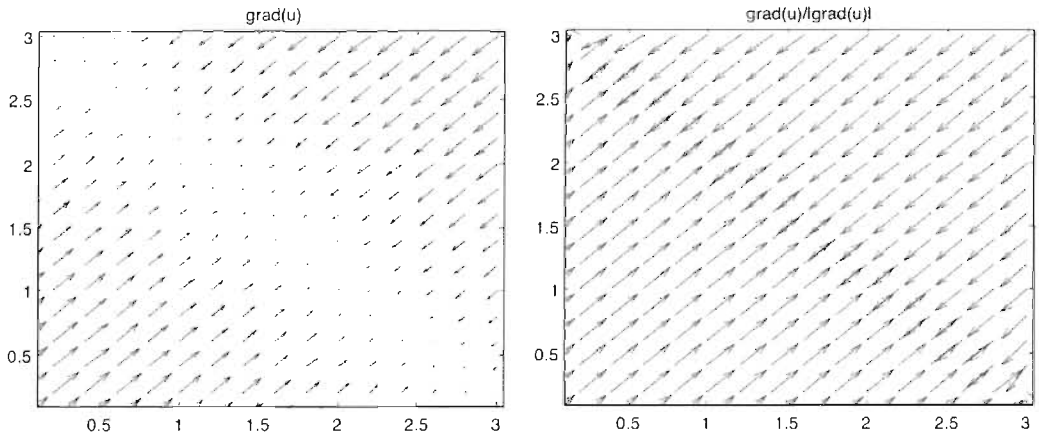

Figure 6.14: Left to right: a plot of ∇u near the maximum of u_0; a plot of $\nabla u/|\nabla u|$ near the maximum of u_0. Note that a discretization of $\nabla \cdot (\nabla u/|\nabla u|)$ would be negative along the maximum.

excess diffusion is faster. See Figure 6.15.

With periodic boundary conditions, we also see faster diffusion. See Figure 6.16.

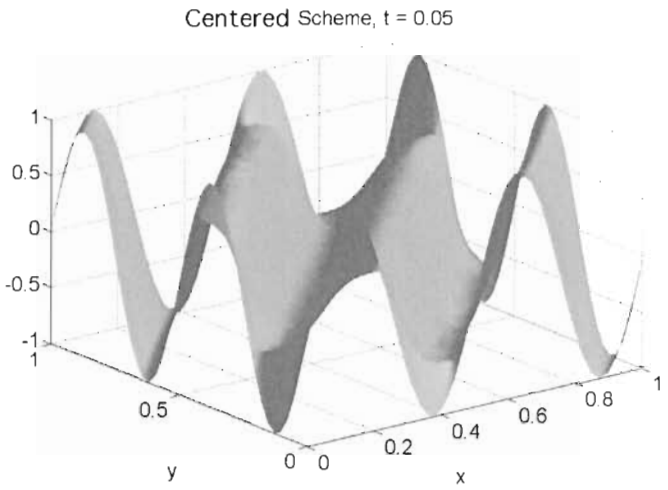

Figure 6.15: The diagonal sine curve test with the centered scheme for grid size 40^2 at $t = 0.05$. Note how the diffusion is faster than that in the results shown in Figure 6.12.

6.3 Steeper Diagonal Sine Curve

We now change the direction of the level sets of the last example to be steeper. Consider the initial condition:

$$u_0 = \sin(2\pi(x - ky)),$$

for integer k. If $k \neq 0$ or ± 1, the level 1 median and morphological schemes can no longer capture the correct solution, since the level sets do not pass through the lattice points on its stencil. If the level set is not captured by the stencil, excess diffusion introduces errors comparable to the initial data. To overcome this, steeper level sets can be captured by stencils of finer directional resolution $d\theta$. For $k = 2$, the level 2 monotone schemes capture the level set direction, while for $k = 3$, level 3 schemes capture. We emphasize that capping occurs for all levels of the median scheme stencils, and not for any morphological scheme stencils.

Figure 6.17 shows results with $k = 3$ for the centered scheme and levels 1, 2 and 3 of the median scheme. Results for the level 3 morphological scheme are shown in Figure 6.18. Note how the centered and levels 1 and 2 median schemes diffuse – they differ from capping. The

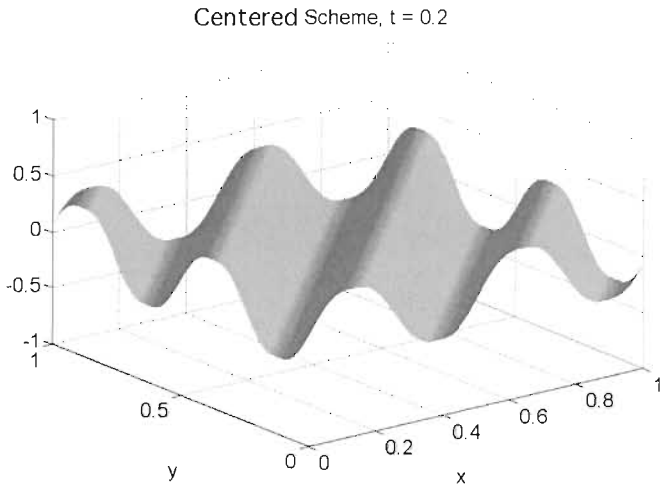

Figure 6.16: The diagonal sine curve test with the centered scheme for grid size 80^2 at $t = 0.2$ with periodic boundary conditions. Note how the diffusion is faster than that in the results shown in Figure 6.12.

level 3 median scheme displays capping, while the morphological scheme does not diffuse.

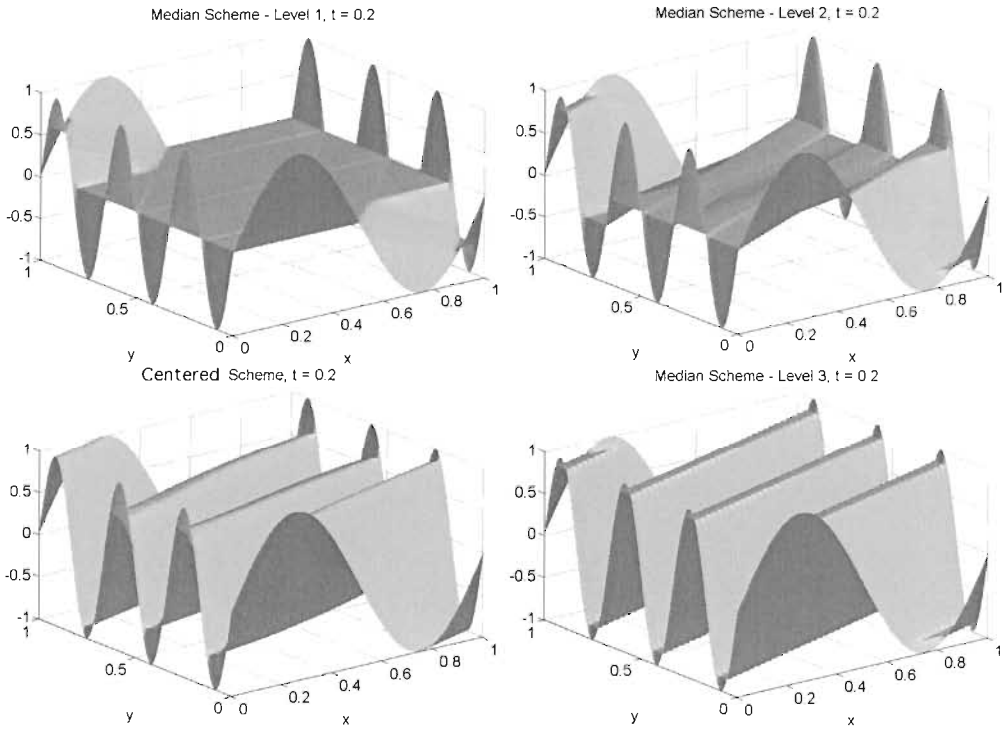

Figure 6.17: Numerical results with initial condition $\sin(2\pi(x - 3y))$ at $t = 0.2$. Clockwise from top left: level 1 median scheme; level 2 median scheme; level 3 median scheme; centered scheme. All computations were performed on a 100^2 grid.

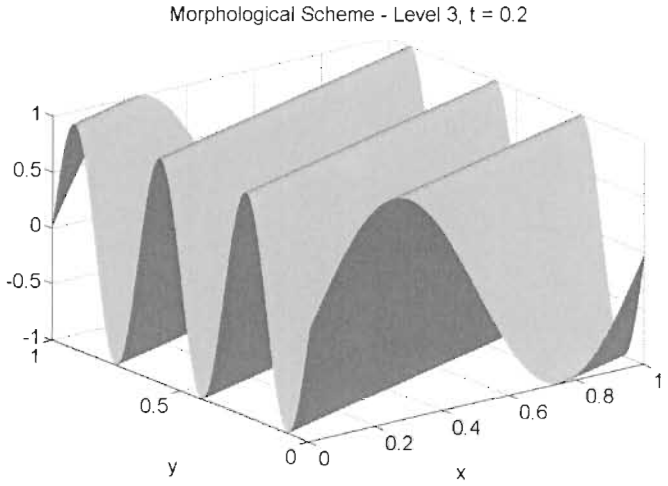

Figure 6.18: Numerical results of the level 3 morphological scheme with initial condition $\sin(2\pi(x-3y))$ at $t=0.2$. Computations were performed on a 100^2 grid.

6.4 The Shrinking Circle

The monotone schemes rely on approximating a circle on a Cartesian grid. We present a weakness due to this approximation. We use the sample viscosity solution

$$u(t,x,y) = \min\left\{\frac{x^2+y^2-1}{2}+t, 0\right\} \tag{6.3}$$

from Example 2.2.3. The level sets of numerical solutions at $t=0.2$ using the median and morphological schemes are shown in Figure 6.19. Note how the level sets are approximately k-gons, where k is the number of lattice points that approximate the circle. The formation of polygonal level sets is inherit to the scheme and does not change with grid spacing dx. The divergence scheme, for example, computes circular level sets - see Figure 6.20.

The ± 0.1 level sets at $t=0.05$ for the monotone schemes and the exact solution are shown in Figures 6.21 and 6.22. Note that the circumscribed approximation of the circle forces the numerical solution to propagate faster than the exact solution. For higher levels of the median scheme, this difference becomes negligible. The morphological scheme, for smaller stencils, experiences similar effects. However, for level 3, the numerical solution propagates more slowly than the exact solution. This is due to insufficient diffusion; this

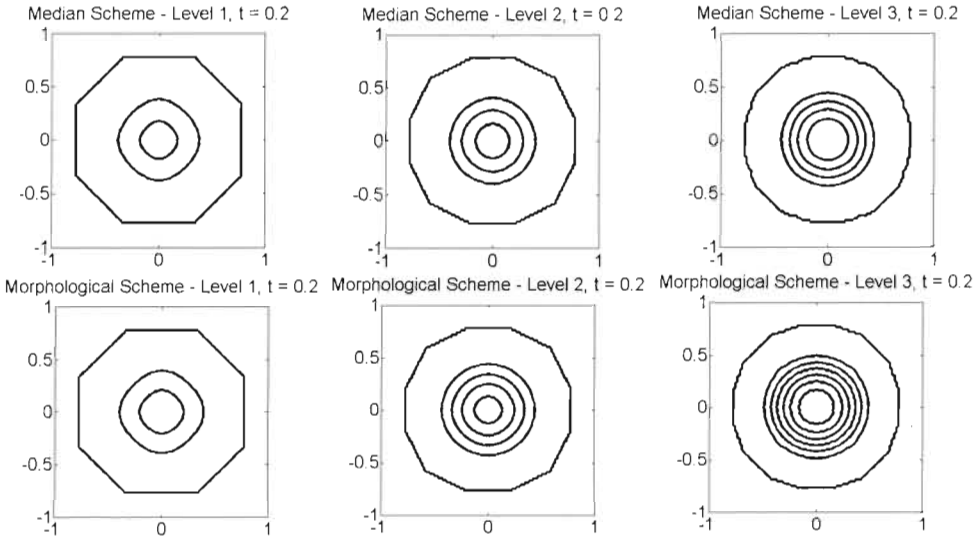

Figure 6.19: Level sets of the shrinking circle by the monotone schemes. Top, left to right: The median scheme level 1, 2 and 3; Bottom, left to right: The morphological scheme level 1, 2 and 3. Computations were performed on a 100^2 grid.

effect is present for all levels of the morphological scheme, but becomes more pronounced as the stencils widen.

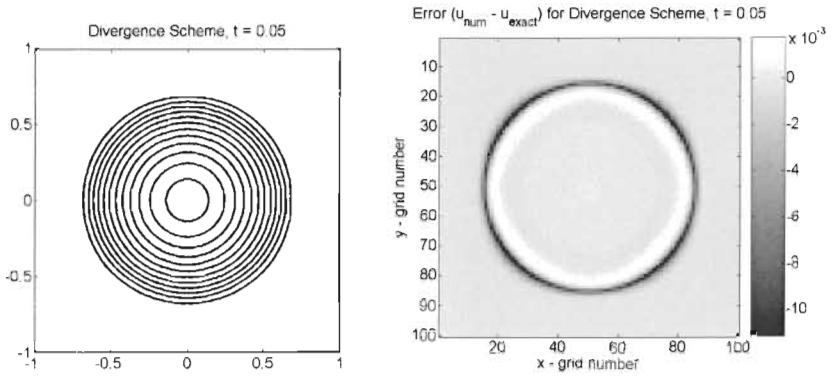

Figure 6.20: Level sets of the shrinking circle by the divergence scheme, and its error relative to the exact solution. Computations were performed on a 100^2 grid.

6.5 Consistency in $d\theta$

As presented earlier, for fixed dx, the convergence rate for both the median and the morphological schemes are $O(d\theta)$ (provided there are no strict extrema for the latter scheme). To confirm this numerically, we again use the exact viscosity solution (6.3) from the shrinking circle test.

We compute the solution at $t = 0.2$ and compare it to the known exact solution. Note that although u is radial with respect to the origin, it is not radial locally, which makes it a good test for directional resolution convergence. We ran the test with the levels 0, 1, 2, 3 stencils for the median and morphological schemes for number of grid points $N = 20, 40, 80$ and 160 on the unit square. We plot the ∞-norm error with respect to $d\theta$. The results are shown in Figure 6.23 for the median scheme and Figure 6.24 for the morphological scheme.

We see that for the median scheme, there is approximately an $O(d\theta)$ convergence as N increases. However, for the morphological scheme, the error from the level 3 stencil is larger than that for the level 2 stencil, due to the insufficient diffusion effect. The plot suggests that the $d\theta$ error dominates for smaller stencils while insufficient diffusion dominates for wider stencils. An interesting result is, the level 2 stencil has a somewhat small max-norm error; this may be due to the two counteracting effects, the circumscribed approximation and the insufficient diffusion, canceling out.

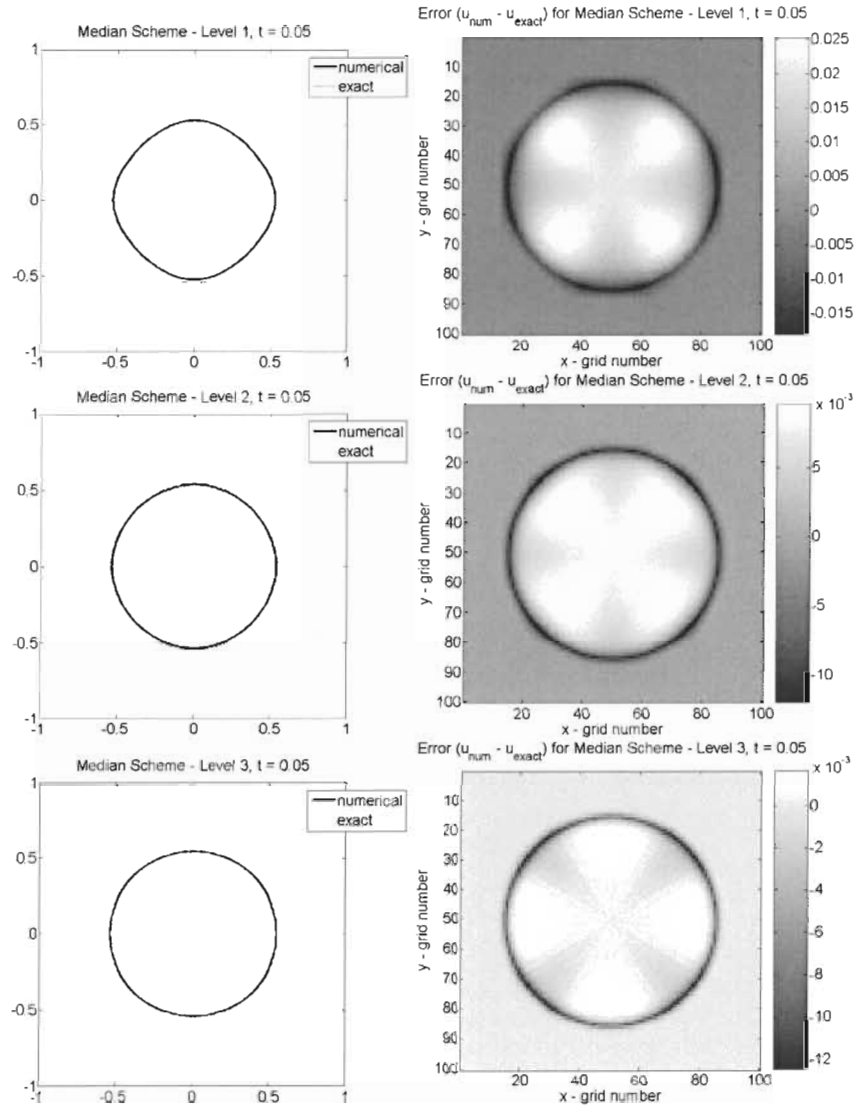

Figure 6.21: The -0.1 level sets of the median scheme (thick) and the exact solution (thin) and the error of the embedding function for the shrinking circle test, at $t = 0.05$. Top to bottom: level 1, 2 and 3. Computations were performed on a 100^2 grid.

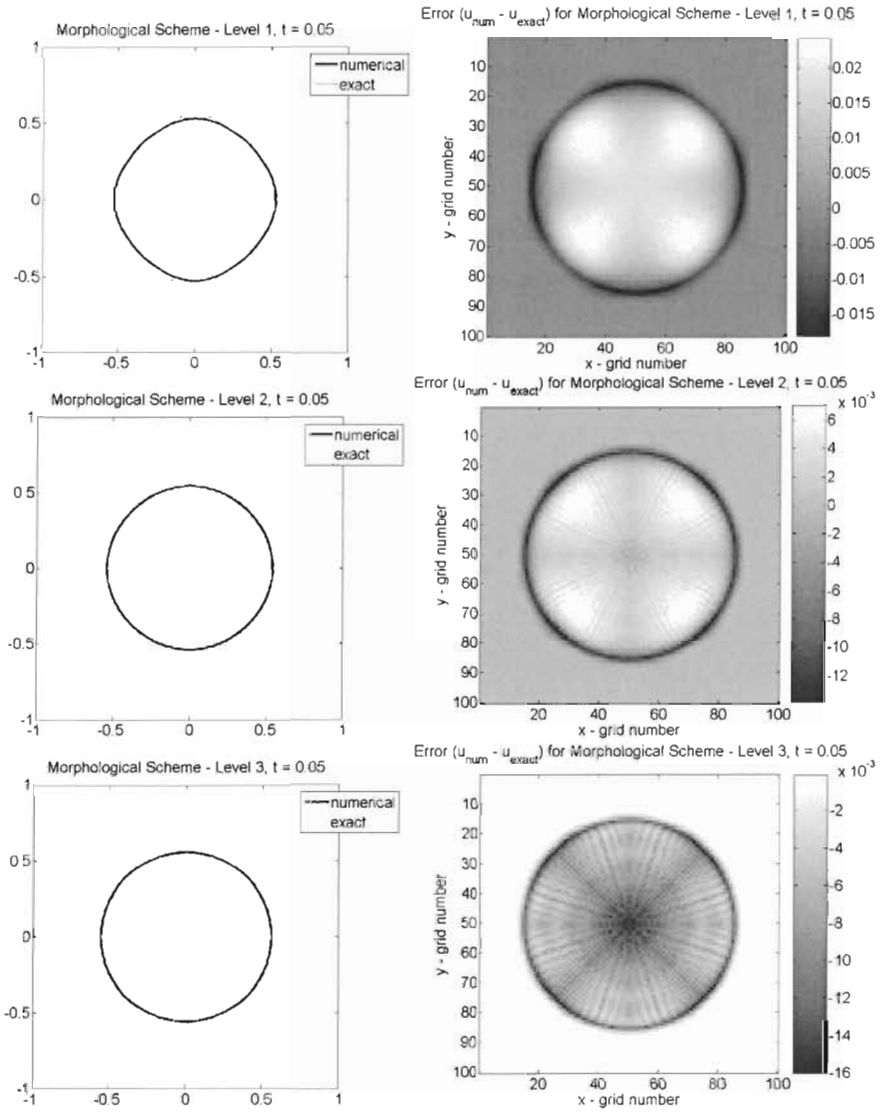

Figure 6.22: The -0.1 level sets of the morphological scheme (thick) and the exact solution (thin) and the error of the embedding function for the shrinking circle test, at $t = 0.05$. Top to bottom: level 1, 2 and 3. Computations were performed on a 100^2 grid.

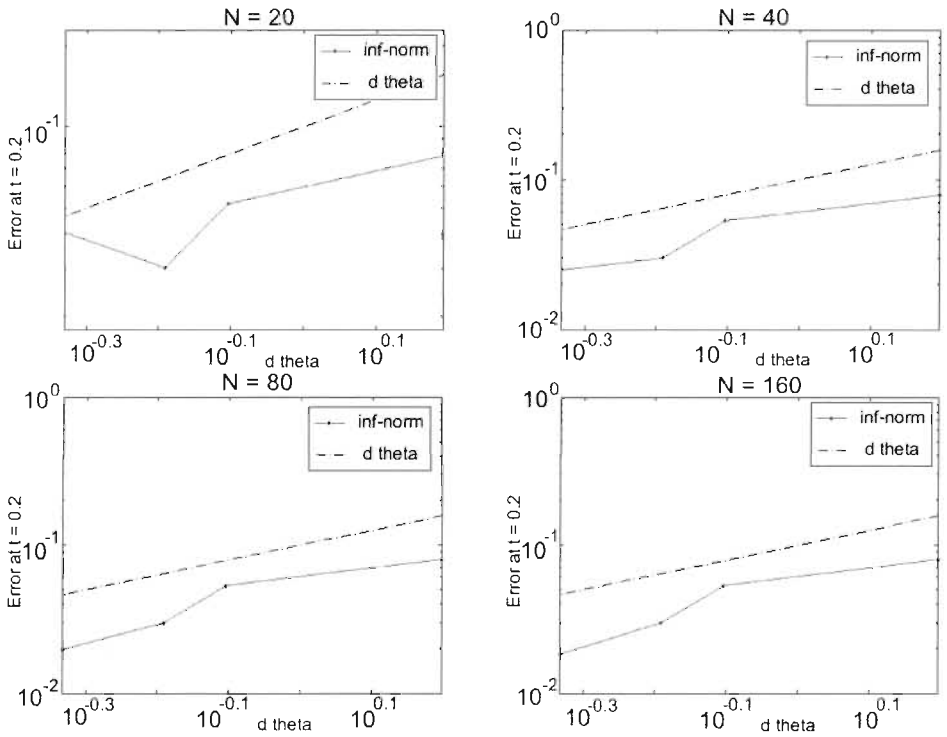

Figure 6.23: Convergence of ∞-norm error with respect to $d\theta$ for various numbers of grid points for the median scheme stencils. Clockwise from top left: $N = 20$, $N = 40$, $N = 160$, $N = 80$. The dotted line represents $O(d\theta)$.

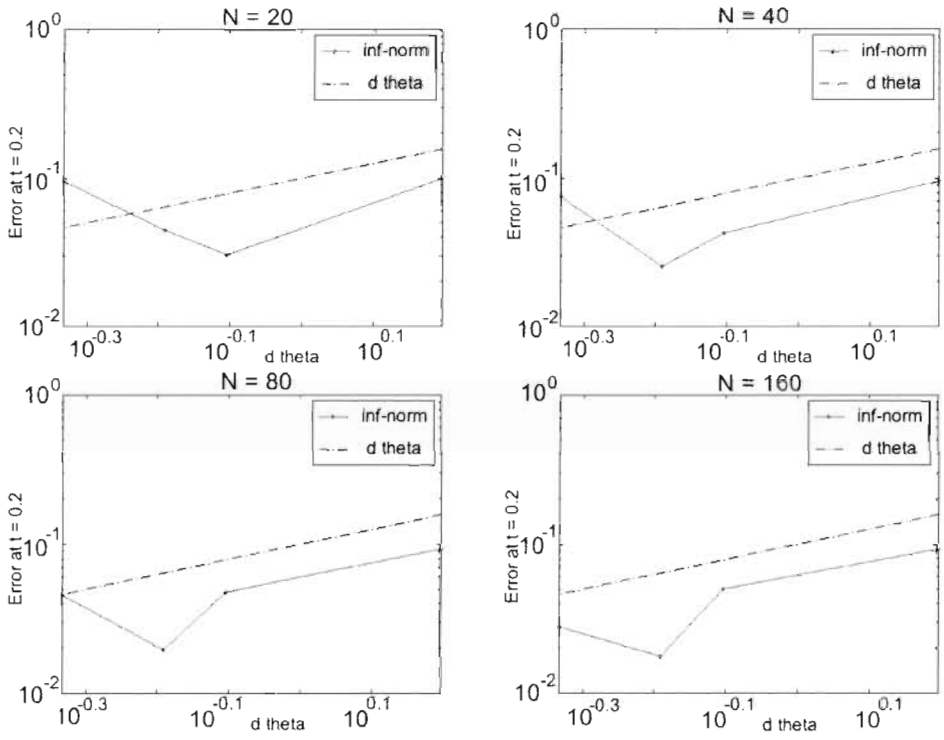

Figure 6.24: Convergence of ∞-norm error with respect to $d\theta$ for various numbers of grid points for the morphological scheme stencils. Clockwise from top left: $N = 20$, $N = 40$, $N = 160$, $N = 80$. The dotted line represents $O(d\theta)$.

6.6 Fattening

The phenomenon of fattening is described in Section 2.3. To reproduce this numerically, we follow the initial condition used in [18]:

$$u_0(x, y) = u(0, x, y) = |x| - |y|.$$

as shown in Figure 6.25.

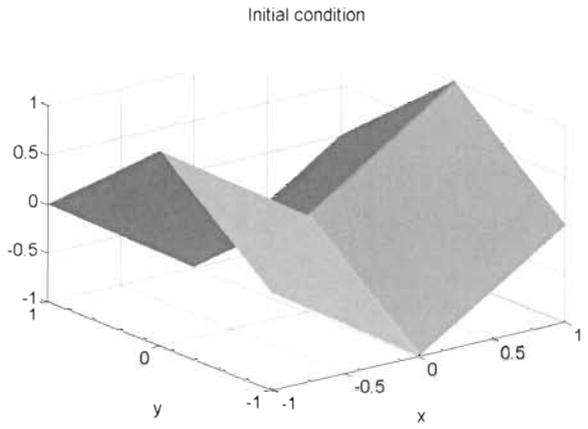

Figure 6.25: The initial condition u_0 for the fattening example.

All nonmonotone and monotone schemes produce the "fat" set of zeros near the origin. We do not know the exact solution explicitly for $t > 0$. We omit the divergence scheme as it produced nearly identical results as the centered scheme. The results are shown in Figure 6.26.

We showed in the diagonal sine curve example that at saddle points, the median scheme produces capping, the centered scheme produces excess diffusion and the morphological scheme produces no diffusion. Moreover, since there are no strict local extrema, the morphological scheme should converge to the unique viscosity solution. The fattening example has saddle points along $y = \pm x$, so we should observe some noticeable differences between the three schemes. In other words, we expect to see the following:

- the median scheme and the morphological scheme should differ by some constant (of $O(dx)$). This is due to the capping of the median scheme at the singularities. This difference should not grow for increasing time, and

- the difference between the centered scheme and the morphological scheme should grow as time increases. This is due to the excess diffusion arising from the centered scheme at the singularities.

The ± 0.01 level sets of the centered, median and morphological schemes at times $t = 0.01$ and $t = 0.5$ are shown in Figure 6.27. Note how:

- at $t = 0.01$, the centered scheme and the morphological scheme level sets are nearly identical, while the median scheme differs from the other two, and
- at $t = 0.5$, the difference between the level sets of the median scheme and the morphological scheme do not change from $t = 0.01$; the level sets of the centered scheme move faster outward, supporting the fact that the centered scheme excessively diffuses.

In other words, for small time, capping gives low accuracy for the median scheme, while for larger time, excess diffusion of the centered scheme grows.

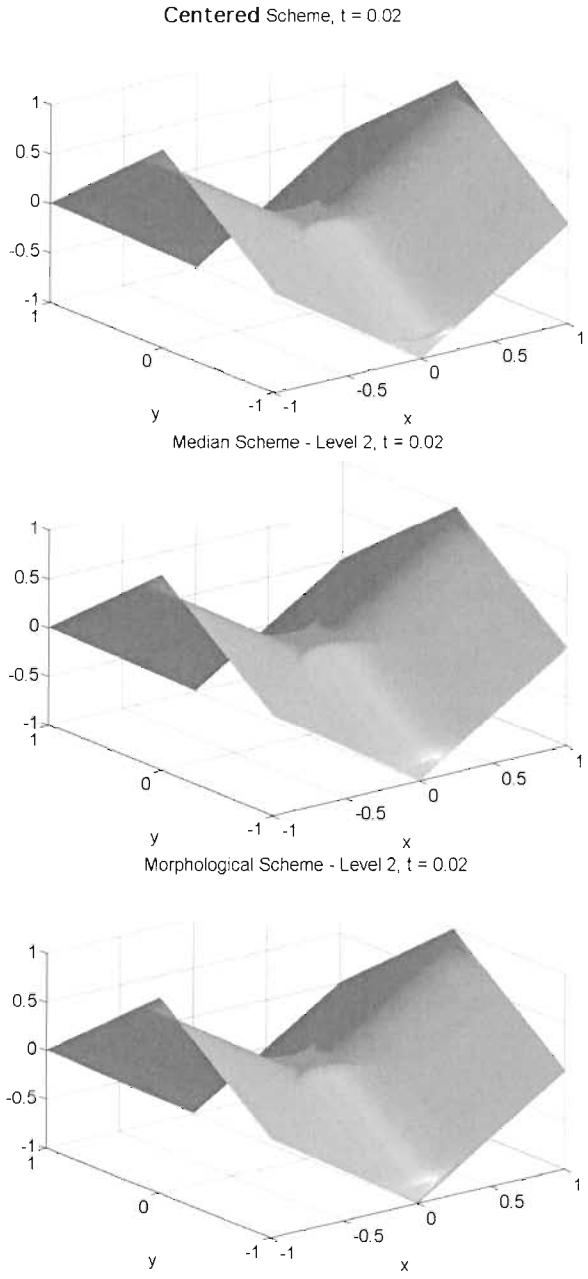

Figure 6.26: Solution at $t = 0.02$ with $u_0(x, y) = |x| - |y|$. Top to bottom: Centered scheme; level 2 median scheme; level 2 morphological scheme. All computations were performed on a 160^2 grid. Note the "fat" set of zeros near the origin for all scheme results.

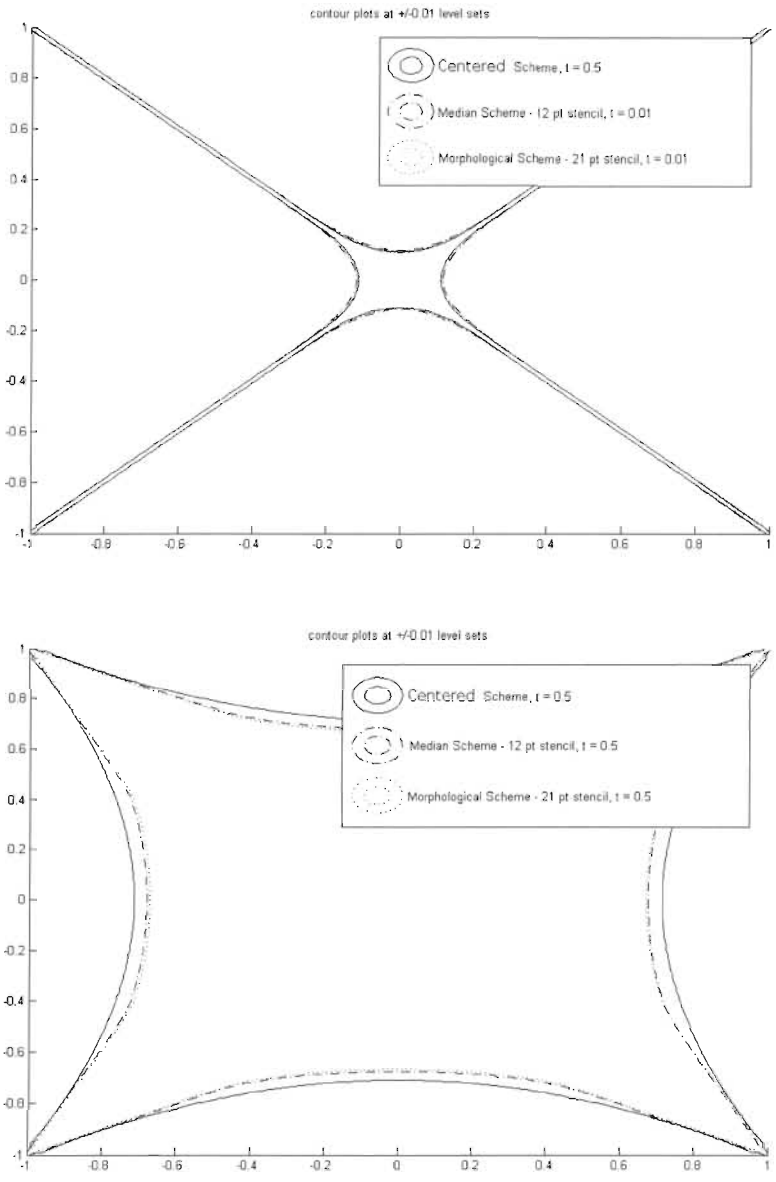

Figure 6.27: The ± 0.01 level sets of the fattening example, computed using the centered, median and the morphological schemes. Top to bottom: the level sets at $t = 0.01$; the level sets at $t = 0.5$. All computations were performed on a 200^2 grid.

6.7 Computational Cost

The nonmonotone schemes in general use far more operations than the monotone schemes. Furthermore, the median and morphological schemes can be simplified into forms (5.9) and (5.16) if $dt = (m \cdot dx)^2/2$ and $dt = (m \cdot dx)^2$, respectively. This is well reflected on the computational cost of the schemes. The time taken to compute the fattening example (Section 6.6) by various schemes are shown in Table 6.1 and Figure 6.28. All computations were done using MATLAB on an Apple PowerMac G5 with 2 GB RAM. The coding for the schemes was optimized by storing as many precomputable values, such as $1/dx$, as possible.

The computational times for the monotone schemes outperform the nonmonotone schemes, largely due to the time stepping. The fastest median and morphological stencils were approximately 10 times faster than the centered scheme and 30 times faster than the divergence scheme. For the nonmonotone schemes, the time step providing stability was chosen by trial and error. For the monotone schemes, the time step increases quadratically as the radius of the stencil. Both monotone schemes therefore performed better as the stencil radius increased, despite the larger number of lattice points in its neighbourhood.

Table 6.1: Computation times in seconds. Med/Morph n refers to the level n Median/Morphological scheme. The nonmonotone schemes used $dt = dx^2/10$ and the monotone schemes $dt = (m \cdot dx)^2/2$, for stability purposes.

Grid	Centered	Div.	Med 1	Med 2	Med 3	Morph 1	Morph 2	Morph 3
20^2	5.35e-3	1.02e-2	5.54e-3	3.96e-4	4.62e-4	3.81e-3	1.16e-3	1.35e-3
40^2	5.53e-2	0.124	4.04e-2	1.21e-2	6.44e-3	7.33e-2	2.67e-2	1.49e-2
80^2	3.96	8.54	0.774	0.338	0.242	1.46	0.583	0.347
160^2	50.9	118	10.9	4.79	4.11	19.2	8.30	5.49
320^2	699	> 1000	198	88.9	70.4	284	121	81.4

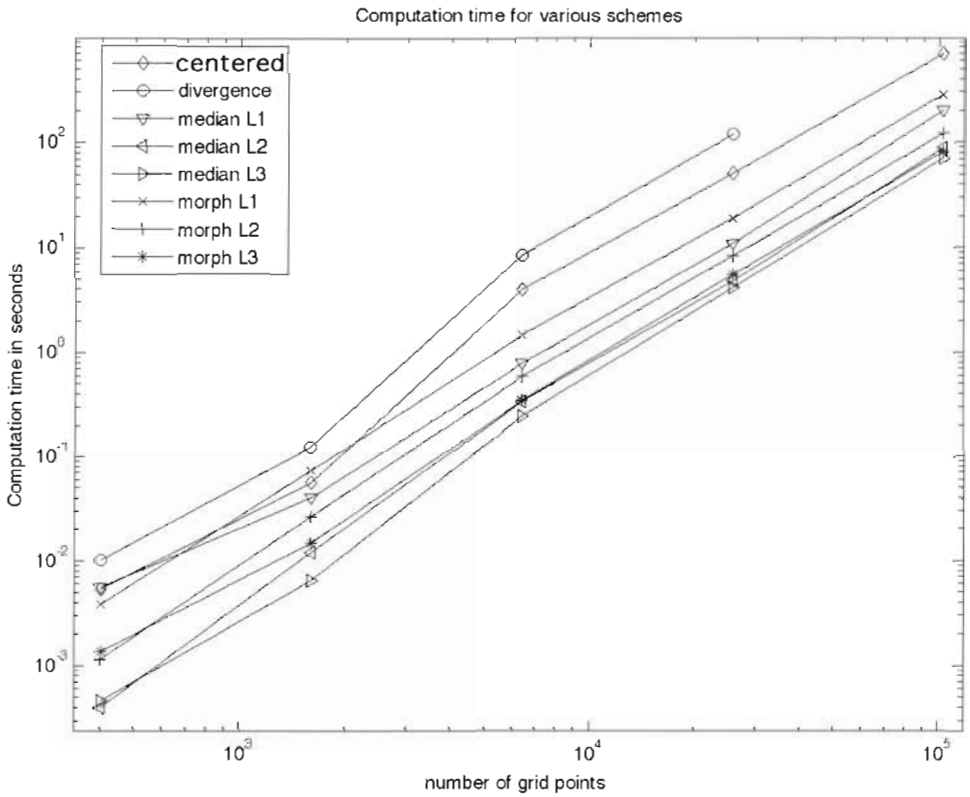

Figure 6.28: Computation times in seconds - the results of Table 6.1 in a log-log graph.

6.8 Closing Remarks

We have presented two degenerate elliptic schemes for solving (1.1): the median and the morphological schemes. We explained that the median scheme converges to the unique viscosity solution for any initial condition, while the morphological scheme converges only in the absence of strict local extrema. The latter scheme therefore experiences insufficient diffusion at strict local extrema, whereas the median scheme does not. Despite this weakness the morphological scheme outperforms the median scheme at saddle points, due to the capping phenomenon. Both monotone schemes compute orders of magnitude faster than the nonmonotone schemes.

Chapter 7

Conclusions and Future Work

In this thesis, we have developed two particular monotone finite difference schemes via three distinct concepts: viscosity solutions, differential game interpretations, and degenerate elliptic numerical schemes. The central conclusions are that the median and the morphological schemes

1. can be interpreted naturally from the differential game interpretation of the motion by mean curvature partial differential equation;

2. outperform traditional finite difference schemes in terms of speed.

In particular, the median scheme always converges to the viscosity solution, despite lower accuracy compared to nonmonotone schemes. Also, nonmonotone schemes may be consistent and stable but not converge to the viscosity solution.

This thesis report is the first to present the connection between the median and morphological schemes to the differential game interpretation of [14]. This is a textbook case of how theory behind an equation provides deeper insight into previously discovered numerical schemes. This may give hope for constructing degenerate elliptic finite difference schemes for other Hamilton-Jacobi equations which have explicit game interpretations.

For future work, it may be interesting to create a hybrid scheme that enjoys the best of both schemes: using the morphological scheme at saddle points to avoid capping, and using the median scheme at strict local extrema to avoid insufficient diffusion. We note that this report does not investigate boundary conditions fully; there may be better choices of stencils near the boundary that work for any problem.

In closing, the median and the morphological schemes have not yet been recognized in the numerical community as much as they may deserve. For example, fast solvers for motion by mean curvature are of importance for computing image processing problems, such as denoising and inpainting, in real time. To the author's knowledge, to date no work in the literature uses either scheme for such applications. We note that a MATLAB toolbox featuring the median scheme has been released by Mitchell [16], [17].

Bibliography

[1] Barles, G., Souganidis, P.E., Convergence of approximation schemes for fully nonlinear second order equations. Asymptotic Analysis, (1991) 4, pp. 271-283

[2] Catte, F., Dibos, F., Keopfler, G., A morphological scheme for mean curvature motion and application to anisotropic diffusion and motion of level sets. SIAM Journal of Numerical Analysis, (1995) 32 (6), pp.1895-1909.

[3] Chen, Y.-G., Giga, Y., Goto, S., Uniqueness and existence of viscosity solutions of generalized mean curvature flow equations. Journal of Differential Geometry, (1991) 33 (3), pp. 749-786.

[4] Crandall, M., Ishii, H., Lions, P.-L., User's guide to viscosity solutions of second order partial differential equations. Bulletin of the American Mathematical Society, (1992) 27 (1), pp. 1-67.

[5] Deckelnick, K., Dziuk, G., Elliott, C.M., Computation of geometric partial dfferential equations and mean curvature flow. Acta Numerica, (2005) 14, pp. 139-232.

[6] Evans, L.C., *Partial Differential Equations.* Graduate Studies in Mathematics, Vol 19, 1998, AMS, Providence.

[7] Evans, L.C., Spruck J., Motion of level sets by mean curvature I. Journal of Differential Geometry, (1991) 33, pp. 635-681.

[8] Fried, M., A level set based finite element algorithm for the simulation of dendritic growth. Computing and Visualization in Science, (2004) 7 (2), pp. 97-110.

[9] Giga, Y., *Surface Evolution Equations. A Level Set Approach.* Monographs in Mathematics, Vol. 99, 2006, Birkhauser, Basel.

[10] Gonzalez, R.C., Woods, R.E., *Digital Image Processing.* 1992, Addison-Wesley, New York.

[11] Grayson, M., The heat equation shrinks embedded plane curves to round points. Journal of Differential Geometry, (1989) 58, pp. 555-557.

[12] Hall, C.A., Porsching, T.A., *Numerical Analysis of Partial Differential Equations.* 1990, Prentice Hall, New York.

[13] Harten, A., Hyman, J.M., Lax, P.D., On finite-difference approximations and entropy conditions for shocks. Communications on Pure and Applied Mathematics, (1976) 29, pp. 297-322.

[14] Kohn, R.V., Serfaty, S. A deterministic-control-based approach to motion by mean curvature. Communications on Pure and Applied Mathematics, (2005) 59, pp. 344-407.

[15] Mao, Y., Comment on motion by mean curvature. Private communication, May 2006.

[16] Mitchell, I. M., The flexible, extensible and efficient toolbox of level set methods. Preprint.

[17] Mitchell, I. M., A Toolbox of Level Set Methods. (2007) UBC Department of Computer Science Technical Report TR-2007-1.

[18] Oberman, A., A convergent monotone difference scheme for motion of level sets by mean curvature. Numerische Mathematik, (2004) 99, pp. 365-379.

[19] Oberman, A., Convergent difference schemes for degenerate elliptic and parabolic equations: Hamilton-Jacobi equations and free boundary problems. SIAM Journal of Numerical Analysis, (2006) 44 (2), pp. 879-895.

[20] Osher, S., Sethian, J.A., Fronts propagating with curvature-dependent speed: algorithms based on Hamilton-Jacobi formulations. Journal of Computational Physics, (1988) 79 (1), pp. 1249.

[21] Rudin, L., Osher, S., Fatemi, E., Nonlinear total variation based noise removal algorithms. Physica D, (1992) 60, pp. 259-268.

[22] Sapiro, G., *Geometric Partial Differential Equations and Image Analysis.* 2001, Cambridge Press, Cambridge.

[23] Sethian, J.A., *Level Set Methods and Fast Marching Methods: Evolving Interfaces In Geometry, Fluid Mechanics, Computer Vision and Material Science*. Cambridge Monographs in Applied and Computational Mathematics, 1999, Cambridge Press, Cambridge.